PHOTOCATALYTIC DEGRADATION OF METHYLENE BLUE DYE WITH GREEN SYNTHESIZED NITROGEN-DOPED ZINC OXIDE

BY

NNODIM, UCHE JUDE

(MENG/SEET/2017/6755)

A THESIS SUBMITTED TO THE POSTGRADUATE SCHOOL FEDERAL UNIVERSITY OF TECHNOLOGY MINNA, NIGERIA IN PARTIAL FULFILMENT OF THE REQUIREMENTS FOR THE AWARD OF THE DEGREE OF MASTER OF ENGINEERING IN CHEMICAL ENGINEERING

JANUARY, 2022

Abstract

The non-biodegradability of organic pollutants and their adverse effects on plant and living organisms makes their removal from the environment vital for the preservation of the ecosystem. In this study, Photocatalysis (one of the advanced oxidation processes) was deployed to remove methylene blue dye (MBD) (a common organic pollutant present in the effluent from textile industries). Green synthesized Zinc oxide (G.S ZnO) precipitates were synthesized from aqueous solution of zinc nitrate hexahydrate and Papaya leaf extracts. The precipitates were dried at 100 ^{o}C for 24 hours, and doped hydrothermally with nitrogen from Urea at different doping ratios (10%, 5% and 2%). Preliminary degradation of MBD with various compositions of Photocatalyst revealed that 5% G.S N-ZnO had superior photocatalytic capabilities than ZnO, 10% G.S N-ZnO, 2% G.S N-ZnO. Effects of solution pH, 5% G.S N-ZnO dosage and initial solution concentration on MBD degradation were studied. An optimum percentage degradation of 83% and 97.5% were observed for ZnO and G.S. N-ZnO photocatalyst at a solution pH of 9.0, MBD solution concentration of 10 mg/L and photocatalyst of dosage of 100 mg per 100 ml of MBD solution. Scanning Electron Microscope (SEM), X-ray Diffraction (XRD), Brunauer-Emmett-Teller (BET) and Fourier Transform Infrared Spectroscopy (FTIR) were used to study morphology, structural properties, surface area and pore volume, and functional groups of Pure ZnO and 5% G.S N-ZnO. FTIR spectra of the 5% G.S N-ZnO was in the range of 4000-500 cm-1, and the ZnO group of G.S N-ZnO was at a low wavenumber. The BET result revealed the surface area of 5% G.S N-ZnO to be 113.3 cm^2/g which was five times that of ZnO. The BET result showed an increase in pore volume and diameter (2.118 nm and 0.055 cm^3/g) of 5% G.S N-ZnO which was greater than that of ZnO (1.452 nm and 0.010 cm^3/g). The shift of the XRD pattern between ZnO and 5% G.S N-ZnO affirms the presence of dopants in the crystalline structure of ZnO. The average crystallite sizes of pure ZnO and 5% G.S N-ZnO were 34.7nm and 24.8nm, respectively. This research revealed that green synthesis and doping could improve the photocatalytic abilities of semiconductor oxides (Zinc oxide), which would increase the efficiency of wastewater treatment using photocatalysts.

TABLE OF CONTENT

LIST OF TABLES

LIST OF FIGURES

LIST OF PLATES

LIST OF ABBREVIATIONS

Advanced Oxidation processes (AOP)

Brunner-Emmett-teller (BET)

Conduction Band (CB)

Energy Dispersive X-ray (EDX)

Fourier Transform Infrared Spectroscopy (FT-IR)

Green synthesized zinc oxide (G.S ZnO)

Green synthesized nitrogen doped zinc oxide (G.S ZnO)

Methylene Blue (MB)

Proton (hv)

Scanning electron microscopy (SEM)

Thermogravimetric analysis (TGA)

Transmission electron microscopy (TEM)

Ultra-violet spectrophotometer (UV-Spec)

Valence Band (VB)

X-ray Fluorescence (XRF)

X-ray Photoelectron Spectroscopy (XPS)

CHAPTER ONE

1.0 INTRODUCTION

1.1 Background to the Study

Pollution is the discharge of untreated waste materials into the surrounding. It is a challenge faced in the world today especially in underdeveloped and developing countries. Pollution is of various types which include land pollution, air pollution and water pollution.

Seventy percent of the earth is made up of water (Marques *et al.,* 2014) and this makes water pollution a serious threat to the survival of mankind. Water pollution is the consistent discharge of untreated industrial/municipal waste into various water bodies. The toxicity of these untreated waste materials make the water unsafe for human consumption. One of the industries that contribute greatly to water pollution is the textile industry (Chen *et al.,* 2017) and the main components of textile wastewater are non-biodegradable dyes. Quantitative and qualitative analysis conducted on textile wastewater in the past revealed that they majorly constitute of organic pollutants. These organic pollutants are recalcitrant, mutagenic, carcinogenic and most times resistant to biodegradation, physical methods and chemical methods (Lawal *et al.,* 2017). A common type of dye found in effluents textile industries is Methylene Blue (MB). Methylene Blue is a cationic dye used in textile industries for various purposes. It is aromatic in nature and has a molecular formula of $C_{16}H_{18}N_3S$. When ingested into the body system of living organisms, it causes genetic diseases and cancer, and it can also result in death (Ullah *et al.,* 2017).

Over the years, various methodologies have been proposed to tackle water pollution by organic pollutants. Among these processes were biological methods also called biodegradation and advanced oxidation processes (AOPs). Advanced oxidation processes were identified as the most economically viable option for degradation of organic pollutants in industrial/municipal wastewater. Advanced Oxidation Processes (AOPs) are of six types and among them, photocatalysis has been identified as the most suitable option for treating wastewater with high concentration of organic pollutants (Saravanakumar *et al.,* 2020).

Photocatalysis is the occurrence of redox reaction in the presence of visible light or ultraviolet light and a photocatalyst. However, Photocatalysis is not without its own drawbacks and one notable drawback is the energy band gap difference between the photocatalyst and light source (visible light or ultraviolet light). Another drawback is the recombination of electron (e^-) and holes pair (h^+) in the valence band. These drawbacks turned the attention of researchers towards other photocatalyst precursors like semiconductor metallic oxide i.e Titanium oxide (TiO_2), Zinc Oxide (ZnO), Tungsten Oxide (WO_3), Iodium (III) oxide (In_2O_3) and Tin Oxide (SnO). Upon several investigations, ZnO was identified as the semiconductor metallic oxide with superior photocatalytic properties because of its light-emitting diodes, good sensor abilities, solar light harvesting and high photo-stability (Ani *et al.*, 2018). This prompted the introduction of doping process into the photocatalyst preparation stage. Doping is the introduction of impurities into a material and recent research studies by (Nguyen *et al.,* 2018) revealed that doping a photocatalyst with appropriate impurity material reduces the energy bandgap difference between the photocatalyst and the visible light region, which in turn makes the photocatalyst active in the visible light region. Material impurities such

as; nitrogen, sulphur atoms, cobalt and graphitic carbon have been identified and explored in past research works for doping.

In the last decade, doping of ZnO with nitrogen has gained much attention and several doping methods have been employed. These methods include; thermal evaporation, thermal nitridation (with ammonia precursor for nitrogen) and hydrothermal methods. Among these methods, hydrothermal demonstrated better advantages because of its simplicity, less time consumption, low energy demands and eco-friendliness. Due to the corrosiveness of the reagents used for the preparation of the photocatalyst, it is pertinent that new processes/methods are incorporated into the photocatalyst preparation stage to make it less hazardous and eco-friendly. In addition, it is also important to improve the efficiency of wastewater treatment through Photocatalysis.

This study presents the synthesis of green synthesized nitrogen doped zinc oxide (GS N-ZnO) as photocatalyst and the degradation of Methylene Blue (MB) dye in synthetic wastewater with photocatalyst (GS N-ZnO).

1.2 Statement of the Research Problem

Discharge of wastewater from process industries poses severe threat to the eco-system due to the presence of carcinogenic and recalcitrant pollutants emanating from industrial effluents. The conventional method transfers pollutants from one medium to another and reusability of the adsorbent or filtrate is often not achievable (Ani *et al.,* 2018). Also, organic compounds are not biodegradable and besides, biodegradation takes longer time. Degradation of highly concentrated organic pollutants under visible/solar is still a challenge in this field of study.

The poor reusability and stability of the photocatalyst is among the setback in the use of heterogeneous photocatalytic processes. The reusability of the photocatalyst could be affected by challenges like the recovery of the catalyst in slurry after use because there are losses during recovery, the deactivation of the active sites by the generated intermediate pollutants or leaching of the active component. Also, degradation of varieties of organic pollutants by a photocatalyst is still a challenge in this field of study. Zinc oxide doped with Nitrogen from Urea and treatment with phyto-chemicals from paw-paw leaf liquid extracts possess the potentials of overcoming the aforementioned affecting the efficiency of heterogeneous photocatalytic process. Creation of heterojunction helps to increase redox ability of the photocatalyst and minimize the leaching of active component of the photocatalyst. With the use of mesoporous high surface area materials engineered with heterojunction, there is high tendency of fast reaction that can degrade highly concentrated pollutants and accommodate more different pollutants at a time due to increased active sites, and the ease of molecular diffusion into the mesopores.

1.3 Aim and Objectives of the Study

The aim of this research work is to degrade methylene blue dye present in effluents from textile industries through Photocatalysis using nitrogen doped ZnO particles enhanced via green synthesis. The aim will be achieved through the following objectives:

i. Synthesis of green synthesized nitrogen doped zinc oxide (GS N-ZnO) from zinc hexahydrate nitrate solution prepared with liquid extracts from paw-paw leaf (carica papaya).

ii. Photocatalytic degradation of the MB dye solution and evaluation of effects of pH, Initial concentration & photocatalyst dosage on percentage the degradation of methylene blue.

iii. Characterization of Nitrogen doped Zinc oxide nanoparticles using *SEM, BET, XRD* and *FTIR* analytical techniques.

iv. Kinetic studies of the Photocatalytic degradation of methylene blue with GS N-ZnO

1.4 Justification of the Study

Advanced oxidation processes do not only eliminate pollutants in wastewater but equally mineralize the pollutants to CO_2 and water.

i. Liquid consumables such as reagents and chemicals aren't required to initiate the redox reactions and this makes Heterogeneous Photocatalysis a cost-effective method for degradation and mineralization of pollutants in the presence of sunlight (renewable energy).

ii. Reusability and stability of a catalyst is one of the key factors considered in industrial application of a catalyst. Catalyst used for heterogeneous Photocatalysis with proper synthesis can be recycled which helps to reduce cost too.

iii. The photocatalyst used are non-toxic and the chemical, thermal and mechanical stability of the photocatalyst makes it even more attractive and suitable for industrial applications.

iv. Operation under a wide range of pH is achievable in heterogeneous Photocatalysis.

v. Complete degradation of organic pollutants which are not biodegradable or have low biodegradability could be achieved.

1.5 Scope of the Study

This research will focus on only degradation of methylene blue dye in synthetic dye solution.

CHAPTER TWO

2.0 LITERATURE REVIEW

2.1 History of Water Pollution

Advancement in technology and increasing world population has led to a corresponding increase in anthropogenic activities, and this threatens water sources around the world. Water bodies have experienced various forms of pollution from various sources and ingestion of water from these contaminated sources has led to diseases such as cholera, typhoid, etc. A recent Cable News Network report states that "one gram of human excreta has 10 million viruses, 1,000 parasite cysts, a million bacteria, and 100 parasite eggs". It is also worth mentioning that in our world today, 1 billion people worldwide can't access safe drinking water and a child dies every 15 seconds from a water-related disease somewhere on the planet (www.water.org).

2.2 Organic Pollutants

Organic pollutants are compounds containing carbon, oxygen and hydrogen as its main constituting elements. They are mostly found in industrial products and waste materials and they are resistant to biodegradation. Due to the recalcitrant nature of organic pollutants, they have tendencies to accumulate on human tissues when ingested into the body system and cause adverse effects on human and the ecosystem in general (Kumar *et al*., 2019). These compounds remain dangerous and active for a long period of time without complete degradation and if unchecked, they can be transported to far distant locations. The menaces caused by these recalcitrant compounds birthed advanced oxidation processes.

2.2.1 Methylene Blue

Methylene Blue (MB) is a synthetic dye commonly used in the Textile industry. It is highly effective for dyeing various materials and its substitute is yet to be discovered (Prabakaran *et al*., 2019). Methylene blue is a heterocyclic aromatic chemical compound with molecular formula of $C_{16}H_{18}N_3S$ and molecular weight of 319.85g/mol. Anthropogenic activities and consistent discharge of untreated wastewater containing traces of methylene blue dye into several water bodies (rivers, oceans, lakes, water channels, etc) has raised a lot of health, environmental and energy conservation concerns globally. This is because methylene blue is carcinogenic and mutagenic in nature and traces of it in living tissues of the human body can causes irreparable damages. Methylene blue is one of the organic pollutants out of numerous organic pollutants that pose serious threats to the ecosystem and past researchers have conducted studies in this area. Mohammed (2019) in his research study attempted to suppress the recombination of electron-hole pairs by adding and studying the synergetic effect of H_2O_2 as an electron scavenger agent on the photocatalytic activity of pod shaped ZnO nanostructures. Subbiah (2019) also studied the effects of micro and nanowires zinc oxides on photocatalytic degradation of MB. Advanced oxidation processes (AOPs) has been identified as the most effective method for treatment of wastewater containing organic pollutants i.e methylene blue (Wang *et al*., 2018).

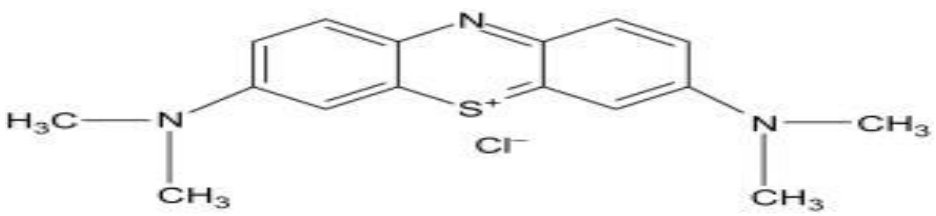

Figure 2.1: Chemical structure of methylene blue (Prabakaran *et al*., 2016).

2.3 Methods for eradicating organic pollutants in industrial wastewater

In the past, several processes have been adopted to tackle water pollution arising from the incessant discharge of organic pollutants into water bodies. These processes include;

2.3.1 Biological processes

Biological processes are processes that employ the use of microorganisms, fungi, green plant and their respective enzymes for the degradation of pollutants/compounds (Megharaj *et.a.l*, 2014). Biodegradation occurs in nature and has been used for decades for purifying contaminated water. The degree and rate of biodegradation of organic compounds is dependent on the constituents of the pollutant. Organic pollutants such as organic matters and organo-phosphorus pesticide can easily be biodegraded. However, some persistent organic compounds such as polyaromatic hydrocarbons (PAHs), heterocyclic compounds, polychlorinated biphenyls (PCBs) and pharmaceutical substances possess high bioaccumulation and biotoxicity properties and these makes them non-responsive to biodegradation under natural condition. Biological process are grouped into two categories. Generally, organic materials are degraded aerobically or anaerobically, explained as follows:

i. **Aerobic biodegradation:** This is the removal of organic pollutants by microorganisms in the presence of oxygen. At the initial stage, microorganisms (fungi and bacteria) produce peroxidases and oxygenases. These compounds then acts as oxidizing agents for the oxidation of organic compounds. In addition, the microorganisms absorb nutrients, carbon and energy released during this process. A large group of microorganisms have the capability of releasing non-special oxidase for degradation of organic pollutants.

ii. **Anaerobic biodegradation**: Anaerobic degradation is removal of organic pollutants by microorganisms in the absence of oxygen. At initial stages, insoluble organic pollutants dissociate to form soluble substances, making them available for other bacteria/fungi to act on (Vermorel *et al.,* 2017). Next soluble organic pollutants which are often sugars and amino acids are converted to CO_2, H_2, NH_3 and organic acid. Acetic acid, CO_2, H_2 and NH_3 are produced from organic acids. The acetic acid is converted to CO_2, H_2 and CH_4 by microorganisms. Anaerobic degradation is inefficient and slow when compared to aerobic degradation. Aside the benefits of COD and BOD reduction during aerobic degradation, renewable energy is also produced (Aljuboury *et al.,* 2017). In addition, the anaerobic bacteria have the potential of breaking down some POPs which are non-responsive to aerobic degradation.

2.3.2 Chemical processes (Advanced Oxidation processes)

Chemical processes are processes designed to remove organic materials in industrial/municipal wastewater through oxidation reactions. Examples of Advanced oxidation processes are; radiation, photolysis, sonolysis, electrochemical oxidation technologies, Fenton-based reactions, UV-based processes, ozone-based processes and Photocatalysis. Some of these processes are explained as follows:

i. Photolysis: Photolysis occurrence of photoreactions in the absence of a photocatalyst. In the past, various research studies revealed that photoreactions could occur in the absence of a photocatalyst, however the amount of organic pollutants removed are often minute, hence the inefficiency of the process. Varadavenkatesan (2019) studied the Photolysis of Diazo dye in an aqueous solution of Metal Nitrate. In the study, the presence of metal nitrates in an aqueous solution changed the photolytic mechanism

and increased the rate of photolysis. From the results obtained, the same amount of decolourization was achieved in a lesser amount of time when 0.15M of Zinc Nitrate was introduced into the reaction medium, hence an increase in photochemical decomposition rate. It was concluded that photolysis functioned best with the introduction of a metallic nitrate into the solution medium because this increased photochemical decomposition rate. Volvoka (2018) also conducted research on the Photolysis of diazo dye in solutions containing zinc and silver nitrates. During the experiment, it was observed that the concentration of diazo dye decreased in the presence of UV radiation. Also, ZnO, ZnO: AgO films and composite coatings with the zinc and silver nitrates further increased the photolytic rate of Chicago Sky blue Diazo dye. It was concluded that percentage degradation of diazo dye increased when the walls of the reaction medium was coated with composite coatings of ZnO and AgO films.

ii. Sonolysis**:** Sonolysis is the use of ultrasonic irradiation for the degradation of organic pollutant. Here, sound waves are used produce hydroxyl radicals (HO^-) in aqueous media. These hydroxyl radicals (HO^-) then act as oxidizing agents for degradation of organic pollutants. Zewde (2019) reviewed the application of the Sonophotocatalytic process based on the advanced oxidation process for degrading organic dyes. Parameters affecting the degradation of organic dyes such as; light intensity, initial dye concentration, catalyst dosage and pH medium were discussed. It was established that low light intensities often prevented the recombination rate of electrons and hence led to increased photocatalytic efficiency and a high electron recombination rate was observed when high light intensities were used. The initial concentration of the organic dye was also observed to affect the degradation efficiency as it was reported that the optimum degradation efficiency was obtained at an initial

concentration of 50 ppm when using TiO_2 as photocatalyst and an initial concentration of 12.5 ppm when using ZnO as photocatalyst. It was established that the counter effect of aggregation of particles and scattering of light energy by the overloaded catalyst led to a decrease in light absorption, which invariably led to a decrease in degradation rate. High degradation rates were observed to occur at a lower pH of the photocatalytic medium. This was because the photocatalyst which has a positive charge will attract more negatively charged electrons, but an increase in the pH of the reaction medium led to the photocatalyst having a negative charge, hence hampering the adsorption of the molecules. It was concluded that combining various advanced oxidation processes, example Sonophotocatalysis had several advantages but Photocatalysis alone is inexpensive, nontoxic, and stable and can be easily reproduced. Siadatnasab (2018) conducted research studies to investigate the performance of $CuS/CoFe_2O_4$ nanohybrid for the degradation of organic dyes. In his research, sound waves were used to produce hydroxyl radicals in the reaction media and $CuS/CoFe_2O_4$ acted as the photocatalyst. The nanohybrid ($CuS/CoFe_2O_4$) was synthesized through hydrothermal method at 200 ^oC and was characterized using the XRD, FE-SEM, EDS, FT-IR, UV-Vis spectroscopy and BET. The efficacy of Sonocatalysis on methylene blue (MB) were observed to be 6%, 62%, 23% using CuS/H_2O_2, CFO/H_2O_2 and $CuS/CFO/H_2O_2$ respectively. Hydroxyl radical was confirmed to be the most prominent oxidizing agent after the addition of a radical hole scavenger (tetra-butyl alcohol). Finally, the reusability and ease of separation of the catalyst were confirmed when a negligible decline in the performance of the photocatalyst was observed after four consecutive runs. Hassani (2017) reported the Sonocatalytic degradation of organic dye using ZnFe-Cl nanolayered as a catalyst. In

the research, ZnFe-Cl exhibited immense potential as a photocatalyst for the degradation of acid red 17.

iii. Electrochemical oxidation: Electrochemical oxidation is occurrence of photoreactions in an electrolytic medium. In a typical set-up, an anode and cathode connected to a power source are immersed into an electrolyte. At the start of the process, energy input is supplied to the electrolyte and this leads to the formation of strong oxidizing species (Cotillas *et al.,* 2018). These strong oxidizing agents then proceed to degrade the organic pollutants. The refractory compounds are thus converted into reaction intermediates and ultimately, into water and CO_2 resulting to complete mineralization. Electrochemical oxidation has recently grown in popularity due to its simple set-up and efficacy in tackling recalcitrant organic compounds/pollutants. It requires no chemical input because the required reactive species are generated at the surface of the anode. It is used to treat a wide variety of non-biodegradable contaminants including aromatics, pesticides, drugs and dyes. However, due to the high energy cost associated with this process, it is sometimes combined with biological remediation to reduce the overall cost of treating organic pollutants. Ali (2019) reported a research study on the degradation of MB dye solution via electrochemical oxidation with Ti/RuO_2-IrO_2 and SnO_2 acting as electrodes. In his study, electrochemical oxidation with Ti/RuO_2-IrO_2 as electrodes was observed to perform better than SnO_2.

iv. Photocatalysis**:** Photocatalysis is the occurrence of a photoreactions in the presence of a photocatalyst. The presence of a photocatalyst during Photocatalysis makes it distinct from Photolysis. Photocatalysis has often been used for the degradation and demineralization of organic pollutants present in wastewater from various process industries such as; textile, pharmaceuticals, oil and gas, paint etc. (Sinar *et al.*, 2020).

Photocatalysis can be heterogeneous and homogeneous depending on the nature of the catalyst in the presence of sunlight or UV light. In Photocatalysis, photons released from the light source falls on the surface of the catalyst.

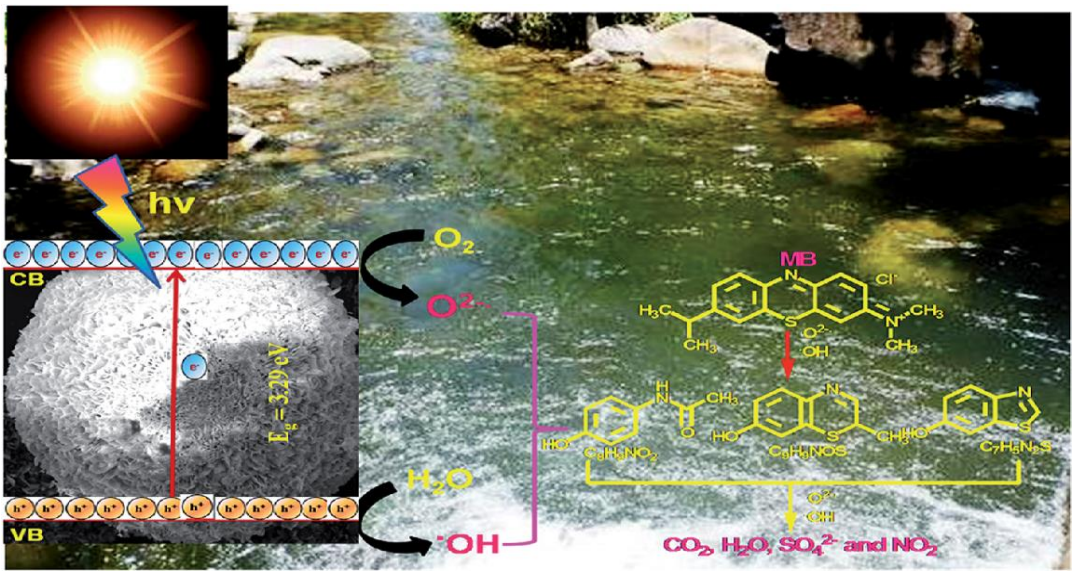

Plate I: Degradation of MB under visible light (Prabakaran *et al.*, 2019)

Plate I present the reaction pathway of Photocatalysis. As the reaction medium containing the photocatalyst and wastewater is exposed to a light source (Visible sunlight or ultraviolet light rays), electrons are excited and moves from the valence band to the conduction band, thereby leaving the valence band with a hold (h^+) and making the conduction band have an electron (e^-). The holes and electrons present in the valence and conduction band then produce O^{2-} and ^{-}OH radicals respectively, and these radicals are the components responsible for the degradation of organic pollutants present in the wastewater. Various studies have been conducted in the area of Photocatalysis and the two major drawbacks are the energy bandgap between the photocatalyst and the light source (visible sunlight) and the recombination of the electron/hole pair at the valence band. These two drawbacks are responsible for reduced degradation of organic pollutants during Photocatalysis. Doping of the photocatalyst with various elements/compounds

such as; nitrogen, carbon nitride, chromium, Iron, etc. has shown tremendous results in the past as it helped lower the difference in bandgap energy between the light source and photocatalyst. In the past, various photocatalyst were used for photocatalytic degradation of organic pollutants in industrial/municipal wastewater and Titanium oxide (TiO_2) has been identified as the most suitable semiconductor metallic oxide for Photocatalysis in the presence of ultraviolet light. However, the high cost of UV-light has turned the attention of researchers to ZnO because of the potentials it possesses. The bandgap energy of Zinc oxide is closest to the bandgap energy of visible sunlight and this makes it suitable for Photocatalysis in the presence of visible light.

Kumar (2019), conducted research on the responsiveness of ZnO nanoparticles (ZnO NPs) for the degradation of methylene blue dye. ZnO NPs was synthesized with zinc nitrate hexahydrate ($Zn(NO_3)_2.6H_2O$) and potassium hydroxide (KOH) through precipitation method. The structural properties of ZnO NPs was studied with X-ray diffraction (XRD) and Raman spectroscopy. The morphology and microstructure was studied through Scanning Electron Microscopy (SEM) analysis. Fourier Transform Infrared Spectroscopy (FT-IR) was then was used to evaluated the functional groups of ZnO NPs. Photocatalytic degradation of methylene blue with ZnO NPs in the presence of solar irradiation was performed and the optimum percentage degradation was obtained to be 95% after 90 mins. Vasiljevic (2020) reported a research study on the photocatalytic degradation of methylene blue (MB) with Titanate nanoparticles (Fe_2TiO_5 NPs) in the presence of sunlight. Fe_2TiO_5 NPs was synthesized via sol-gel method and calcined at 750^oC. Photocatalytic degradation experiments were then conducted on MB and the effects of solution pH, initial concentration and photocatalyst dosage was studied. The optimum percentage degradation was recorded to be 97% at pH = 11 and initial

concentration of 100 mg/L. The morphology, bandgap energy and surface area of Fe_2TiO_5 NPs were studied with XRD, UV-Vis absorbance spectra and BET analysis. It was concluded that Fe_2TiO_5 NPs possess immense photocatalytic abilities and could efficiently serve as a photocatalyst for treatment of MB in wastewater treatment.

Kwon (2020), conducted research on synthesis of silver doped ZnO (Ag-ZnO) for the photocatalytic degradation of Methylene blue in the presence of sunlight. Different ratios of Ag-ZnO were prepared through hydrothermal methods and were used to perform degradation of MB. It was observed that a photocatalyst with 0.1% mol Ag in Ag-ZnO exhibited better performance that other Ag-ZnO photocatalyst having 0.2% mol, 0.3% mol, 0.4% mol and 0.5% mol of Ag. The morphology, crystallinity and surface properties of the Ag-ZnO were studied with FE-SEM, XRD and XPS (X-ray photoelectron spectroscopy) techniques respectively. It was concluded that 0.1% mol of Ag in Ag-ZnO gave the optimum percentage degradation of 92.9% for the MB. Asman (2020) conducted research on the synthesis of egg shell based activated carbon for the photocatalytic degradation of Methylene blue in the presence of UV-Visible irradiations. Egg shells were obtained, milled and pretreated with separately two different reagents; Orthophosphoric acid (H_3PO_4) and Sodium Hydroxide (NaOH). The pretreated powdery egg shells were then washed with dilute water and calcined at 550 ^oC for 3 h. Photocatalytic degradation experiments on methylene blue was conducted differently for both samples (egg shells pretreated with NaOH and Egg shells treated with H_3PO_4) and it was observed that egg shells treated with H_3PO_4 exhibited a percentage degradation of 83% which was greater than its counterpart (egg shells pretreated with NaOH) which exhibited a percentage degradation of 74%. The optical, electronic and physicochemical properties of both solid samples were studied using X-ray diffraction (XRD), Fourier

Transform Infrared Transform (FT-IR) and Scanning Electron Microscope (SEM). It was established that photocatalytic degradation of organic pollutants by activated carbon from egg shell based materials gave 83% degradation of methylene blue dye and this could be applied for wastewater treatment on an industrial scale. Saravanakumar (2020) conducted the photocatalytic removal of anionic and cationic dyes in textile effluents by H_2O_2 assisted titanium oxide (TiO_2) and micro-cellulose (MC) composites. In his research, TiO_2 + MC composite was synthesized by two steps; pre-treatment of banana fibre and mixing of banana MC fibres with a solution of CH_3COOH, C_2H_5OH & $C_{12}H_{28}O_4Ti$. The TiO_2 + MC composite was used as photocatalyst for the degradation of methylene blue (MB), methylene violet (MV) and acid violet (AV). Effects of solution pH and catalyst dosage were studied and the optimum percentage degradation (93%) was obtained when pH, catalyst dosage and initial concentration were 7.0, 0.1g/L and 200mg/L respectively. In conclusion, TiO_2 + MC composite was recommended as a suitable photocatalyst for the photocatalytic degradation of organic pollutants present in effluents from textile industries.

Sun (2020) conducted research on the synthesis of N self-doped ZnO. In his research, nitrogen doped zinc oxide (N-ZnO) was synthesized from a metallic organic framework (MOF) called zeolite imidazole (ZiF). He first prepared three samples of ZiF (M-Zif-8, S-Zif-8 & P-Zif-8) with zinc nitrate hexahydrate ($Zn(NO_3)_2.6H_2O$), 2-methylimidazole (Hmim) and sodium formate (HCOONa) through three routes; microwave hydrothermal method, solvothermal method and precipitation method. The proposed photocatalyst (self-doped N-ZnO) was then prepared by calcining each of the three ZiF samples (M-Zif-8, S-Zif-8 & P-Zif-8) for 2 hours at a temperature of 550^oC, and three samples of self-doped N-ZnO were obtained and labeled as M-ZnO-550, S-ZnO-550 and P-ZnO-550.

Photocatalytic activities was preceded by adsorption-desorption process in the presence of the photocatalysts (M-ZnO-550, S-ZnO-550 and P-ZnO-550) and in the absence of solar-irradiation. It was observed that each photocatalyst had 5% adsorption efficiencies. The photocatalytic degradation experiment was then conducted for 80 min for each photocatalyst (M-ZnO-550, S-ZnO-550 and P-ZnO-550). M-ZnO-550 exhibited higher photocatalytic degradation efficiency (95.3%) than P-ZnO-550 (90.8%) and S-ZnO-550 (91.8%). The three samples of the photocatalyst (M-ZnO-550, S-ZnO-550 and P-ZnO-550) plus pure commercial ZnO was studied and the distinct difference between the properties of the three photocatalyst and commercial ZnO confirmed the efficacy of the microwave hydrothermal doping method. The higher photocatalytic degradation efficiency by M-ZnO-500 and the less time required to synthesize M-ZnO-550 affirmed it is best suitable than P-ZnO-550 and S-ZnO-550 for degradation of MB in wastewater treatment. This implied that microwave hydrothermal technology possess an immense potential in the area of Photocatalysis.

Tichapondwa (2020) from the department of Chemical Engineering, University of Pretoria South Africa conducted research on the photocatalytic performance of three commercial TiO_2 powders (Degussa p25 TiO_2, pure Anatase and Rutile) with different crystal phases as Photocatalyst. The optical, electronic and physicochemical properties of each photocatalyst was studied with the XRD, BET, FTIR and SEM. Photocatalytic degradation experiments on phenolic methylene blue (MB) were then conducted using each Photocatalyst and it was observed that Degussa p25 TiO_2 exhibited better photocatalytic performance than pure Anatase and Rutile samples. Optimization studies for degradation of phenolic MB and 95% degradation was achieved at a Photocatalyst loading of 0.5g/L and pH of 10. Effects of doping on the photocatalytic performance of

Degussa p25 TiO_2 was also studied and it was observed that percentage degradation increased by 2% for copper dopant but decreased by 5% for zinc dopant. It was concluded that Degussa p25 TiO_2 had the potential of being deployed as an efficient photocatalyst for wastewater treatment at commercial scale.

Golmohammadi (2019) carried out research studies on the synthesis of green synthesized zinc oxide nanoparticles (ZnONPs) for the photocatalytic degradation of organic dyes (methylene blue and eriochrome black-T). Jujube plant leafs were obtained from a nearby garden and dried. It was then crushed and 50 grams of the powdery form of dried Jujube plant was soaked and boiled to obtain the liquid extract. The liquid extract from Jujube plant leaf was used as the solution solvent during the synthesis of ZnO nanoparticles through hydrothermal method. Photocatalytic degradation experiments were conducted on dye solution with green synthesized ZnONPs acting as a photocatalyst. The experiment yielded 92% degradation of MB dye and 86% degradation of ECBT. Reusability studies conducted with ZnONPs revealed a minute decrease in percentage degradation of both organic pollutants after four cycles. The morphological, electronic and physicochemical properties of the ZnONPs were studied with analytical techniques like TEM, SEM-EDX, FTIR and XRD analysis. In conclusion, it was proposed that green synthesized ZnONPs has the potential of efficiently acting as a photocatalyst for the degradation of organic pollutants during wastewater treatment systems.

Muhammad (2020) conducted research on the synthesis of green synthesized zinc ferrite nanoparticles (ZF- NPs) for the degradation of methylene blue (MB) dye. Liquid extracts from Piper Nigrum seeds were used as solvent for the synthesis of ZF- NPs. Zinc nitrate hexahydrate and hydrated iron nitrate were used as the precursors for the ZF- NPs and

hydrothermal procedure was used for this step. Degradation of MB with green synthesized ZF- NPs was conducted and the influence of catalyst dosage and initial solution concentration on percentage degradation was studied. The catalyst was characterized with FTIR, SEM, FE-SEM, XRD and TGA and it was observed that ZF-NPs had enhanced photocatalytic abilities. In conclusion, ZF- NPs was proposed as a suitable Photocatalyst for the degradation of MB in wastewater treatment on an industrial scale.

Messih (2019) conducted research on the synthesis and characterization of silver doped zinc oxide (Ag-ZnO) nanoparticles for the degradation of methylene blue in the presence of UV and visible sunlight. Zinc nitrate hexahydrate and silver nitrate were used as precursors to prepare several Ag-ZnO samples with 0 - 5 wt% Ag through sol-gel chemical method. The morphology, crystallinity and electronic properties of Ag-ZnO were studied with SEM, XRD and XPS respectively. Photocatalytic activity of the four samples of Ag-ZnO was carried out and 3wt% Ag-ZnO exhibited the best performance. Kinetic study was also conducted for each of the four Ag-ZnO samples and 3wt% Ag-ZnO had the highest rate constant and lowest half-life. In conclusion, it was proposed that 3wt% Ag-ZnO be deployed as a Photocatalyst for degradation of organic pollutants in wastewater treatment systems.

Rowshon (2020) conducted research on synthesis of nitrogen doped ZnO nanoparticles for the degradation of Methylene blue in the presence of visible light. Zinc acetate dihydrate, oxalic acid and urea were used for the synthesis of nitrogen doped zinc oxide nanoparticles. Photocatalytic degradation of Methylene blue and Rhodamine B were performed and it was observed that N-Doped ZnO exhibited better photocatalytic

performance than pure ZnO under the same condition (visible sunlight). N-Doped ZnO nanoparticles was examined with analysis like Fluorescence Spectroscopy, FTIR, XRD, SEM and UV-Vis-NIR spectroscopy. XRD revealed the crystal sizes of pure and N-doped ZnO to be 29nm and 28nm. The UV-Vis-Spectroscopy revealed that the transmittance of N-Doped ZnO was visible and infrared of N-Doped ZnO was higher than pure or undoped ZnO. An optimum percentage degradation of 98.11% for MB was using N-Doped ZnO as Photocatalyst and 86.21% for RB was reported too, which were higher than the percentage degradation reported for pure or undoped ZnO. It was concluded that doping of photocatalytic material enhanced their photocatalytic capabilities and led to a higher percentage of degradation in wastewater treatment using Photocatalysis.

Amita (2019) conducted research on synthesis of cobalt doped nickel oxide (Co-N_iO) nanoparticles for Methylene blue degradation in the presence of visible light. It was observed that percentage degradation under visible light was greater than percentage degradation under UV light for all the three parameters (pH, initial concentration and catalyst dosage). Characterization of the Co-NiO nanoparticles were carried out by conducting Fluorescence Spectroscopy, Fourier Transform Infrared Spectroscopy (FTIR), X-ray diffraction (XRD) and Scanning Electron Microscopy (SEM) analyses. Nitrogen doped ZnO nanoparticles catalyst demonstrated improved photodegradation efficiency of 94% visible light irradiation in 50 min. It was concluded that doping of photocatalytic material enhanced their photocatalytic capabilities and led to a higher percentage of degradation in wastewater treatment using Photocatalysis.

Prabakaran (2019) conducted research on synthesis of nitrogen doped ZnO nanoparticles for the photocatalytic degradation of Methylene blue in the presence of UV and visible

light. It was observed that percentage degradation under visible light was greater than percentage degradation under UV light for all the three parameters (pH, initial concentration and catalyst dosage). Nitrogen doped ZnO nanoparticles were characterized FTIR, XRD, Raman Spectroscopy, Thermogravimetric Analysis (TGA), SEM, TEM, Electron Dispersive Spectroscopy (EDS) and EDX elemental mapping. Nitrogen doped ZnO nanoparticles catalyst demonstrated improved photodegradation efficiency of 98.6% and 96.2% under visible and UV light irradiation at different time intervals. It was affirmed that Nitrogen doped ZnO nanoparticles were reusable and percentage degradation of 93.2% was recorded after four cycles. It was concluded that doping of photocatalytic material enhanced their photocatalytic capabilities and led to a higher percentage of degradation in wastewater treatment using Photocatalysis.

Huo (2018) performed photocatalytic degradation of organic pollutants by ZnO modified TiO_2 nanocomposites. In his research, various ratios/proportions of ZnO-TiO_2 nanocomposites were prepared through impregnation-calcination method and they were used for the degradation of organic pollutants in salicylic wastewater. It was observed that 7% Zn-TiO_2 exhibits much better than their pure ZnO and TiO_2. Total organic carbon (TOC) removal efficiency was also studied using 7%Zn-TiO_2 and it was observed that 7% Zn-TiO_2 had better performance than pure ZnO and TiO_2 separately. Reusability test for 7%Zn-TiO_2 was conducted and 7%Zn-TiO_2 proved to be highly stable in the photocatalytic ozonation process after four cycles. It was also observed that the photocatalyst can be active within a pH range of 0.5 to 10.0. In conclusion, it was established that 7%Zn-TiO_2 nanocomposites had immense potential for treating wastewater containing organic pollutants.

2.4 Basic properties of good photocatalyst

Ahmed (2017) reports that ZnO nano particles (NPs) can exist in solid phase or as a liquid suspension. Regardless of the phases involved, a number of factors is considered for a catalyst to be regarded as a good photocatalyst. These includes;

i. High surface area
ii. Good photo-stability
iii. Appropriate band gap
iv. High carrier mobility
v. Correct band-edge positions
vi. Efficient light absorption

Also, the authors justified the use of photocatalysis in wastewater degradation due to the following reasons:

i. Active species
ii. Reactions take place at room temperature and pressure
iii. Re-use of photocatalyst is guaranteed
iv. No need for post processes
v. No consumption of expensive oxidizing chemicals
vi. Applicable to both slurry and immobilized reactors
vii. Regeneration prospect

2.5 Zinc Oxide (ZnO) Photocatalyst

ZnO is widely acclaimed to have a bandgap of 3.21 eV with a high binding energy (60 meV) (Vishnukumar *et al.*, 2018). Zinc oxide (ZnO) is recently considered to be among the most significant binary II–VI compounds with wurtzite structure (Byzynski *et al.*, 2017). It is reported to have the attention of researchers owing to its exceptional

properties and multipurpose applications in diodes (Wang *et al., 2*015), solar cells (Lupan *et al.*, 2010), transparent conducting electrodes (Mhamdi *et al.*, 2015), gas sensors (Biasotto *et al.,* 2014), laser diodes and thin film transistor (Wang *et al.,* 2018). Different methods have successfully produced ZnO thin film such as spray pyrolysis, RF sputtering, sol–gel method amongst others (Ibrahim *et al.,* 2013). As an alternative to TiO_2, ZnO has been reported as an effective catalyst, although researches have also been conducted using ZrO_2, SrO_2 and CdS. ZnO as reported by Wang *et al.,* (2018) possesses unique properties that is relevant in several applications, notable among the are solar cells, transparent conducting films, ultraviolet lasers, and photocatalyst. It has recently been reported that micrometer-sized hollow structures of zinc oxide (ZnO) have enticed majority of researchers as photocatalysts because of their low cost, applicable flat band potential high electron mobility, environmental friendliness as well as environmental sustainability (Wang *et al.,* 2017).

2.6 ZnO structure

According to Lee (2015), ZnO has a well-defined crystal wurtzite or cubic (zinc blende) structures which are normally in rock salt. The rock salt structure of ZnO is produced at intense pressure making its structure uncommon. Thermodynamically, of the three structures, wurtzite structure of ZnO which is the most common has the best stability. ZnO crystal structure is hexagonal wurtzite at ambient temperature and pressure, having two lattice constants values approximately 0.3 nm and 0.5 nm (Baruah and Dutta, 2009). Figure 2.2 exhibits the structures of ZnO; it can be detected that the wurtzite ZnO contains atoms developing hexagonal-close pack sub-lattices which will stack alternatively along the *c*-axis. When situations of this kind occur, it will be observed that each Zn^{2+} sub-lattice contains four Zn^{2+} ions and surrounded by four O_2^- ions and vice versa, coordinated

at the edges of a tetrahedron. Similarly, the tetrahedral coordination produces polar symmetry along the hexagonal axis. This polar symmetry creates spontaneous polarization which is an important parameter affecting ZnO crystal growth in the cause of synthesis.

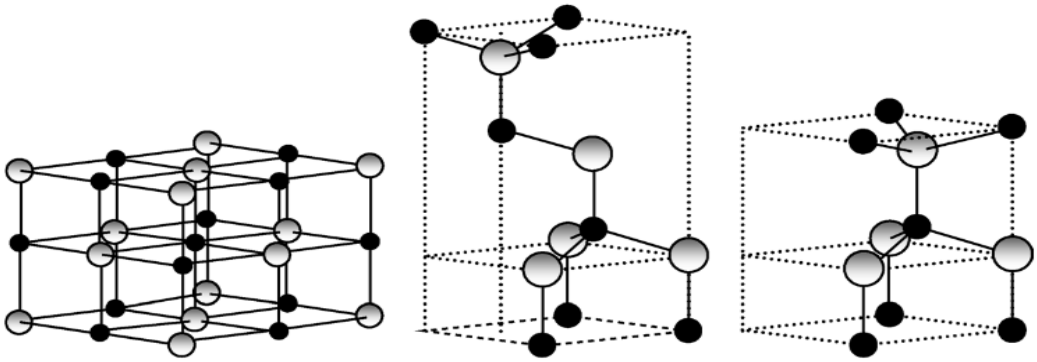

Figure 2.2: ZnO crystal structures from left to right (a) cubic rocksalt; (b) cubic zincblende; (c) hexagonal wurtzite. The larger and smaller spheres denote Zn and O atoms respectively (Lam *et al*., 2012)

2.7 Challenges of ZnO as photocatalyst

Researchers in photocatalysis ultimately desires at all times to design as well as to fabricate photocatalyst that possesses suitable band structure, good redox potential, high photoactivity at visible region and good stability. Sadly, these are still the challenging practices in the world of photocatalyst synthesis and activity. It is also true that in the conventional processes, the inadequate solution to recombination and/or the inability to absorb light rays in the visible region are inevitable problems associated with photocatalysis. Nevertheless, much efforts have been devoted to bringing these limitations to check. Remarkably and irrespective of its resourcefulness, ZnO photocatalyst is still not devoid of challenges. Most notable amongst these challenges are

detailed below (Wang *et al.*, 2017, Samadi *et al.*, 2016, Kumar *et al*., 2017, Pirhashemi, *et al.*, 2018).

(a) The ineffectiveness of ZnO photocatalyst is because of the characteristic broad band gap. As a result, the catalyst can only absorb limited portion of the energy beam from the sun (3–5%).

(b) ZnO photocatalyst is also known for the spontaneous recombination of the photo-induced charge carriers which limits them from getting to the surface, thereby resulting in reduction of the reactions that are known to occur on the liquid interface/semiconductor; and

(c) ZnO photocatalyst is highly rated in terms of photo-corrosion when exposed to irradiation. Furthermore, ZnO dissolves in acidic and alkaline solutions; though reactions are favored in the later.

Consequently, pure ZnO photocatalyst have not been able to meet up to the projection of researchers on photoactivity under natural sunlight. To this end, extensive researches have been geared up to improving photo-catalytic activity of ZnO by overcoming the known drawbacks encountered as photocatalyst. Interestingly, several researches are currently working on how to improve the visible light response of ZnO based photocatalyst by applying techniques like: creation of hetero-junctions between semiconductors, band gap narrowing through the integration of ZnO with metal/non-metal dopants, amongst others. Numerous insightful and useful researches on the analysis of these strategies are documented reported extensively (Pirhashemi, *et al.,* 2018, Selvin *et al.*, 2017, Adhikari *et al.,* 2014, Anirudhan & Deepa, 2017).

2.8 Strategies to better the photodegradation efficiency of ZnO

The major obstacle commonly associated with photocatalysis is the inability to withstand for long the charge separations of photogenerated hole (h^{VB+}) and electron (e^{CB-}). This recombination step causes energy wasting and lowers the quantum yield. To remove this setback, the e^-/h^+ recombination must be subdued to guarantee effective photocatalysis. The use of dopants could solve the problem of recombination by introducing barriers for the electrons and holes to remain separate. Subsequently, the dopants may hinder electrons thereby decreasing the chances of electron-hole combining again. In addition, intermediate species like hydroxyl and superoxide radicals generated will highly improve the charge separation efficiency. On a wider note, nature and dopant ratio, operating parameters and synthesis method significantly affect the photo-effectiveness of doped photocatalyst (Lee *et al.,* 2015).

2.9 Green Synthesis

Green synthesis is a methodology research that has gained so much attention in the past few years. In Photocatalysis, it involves the synthesis of nanoparticles (photocatalyst) with liquid extracts from a plant leaf. The procedures for the preparation of photocatalyst for Photocatalysis has been known to be unsafe/hazardous, hence the need to incorporate an environmentally safe additional procedure to make the photocatalyst stage safe. Fungi, Plants, stems and root liquid extracts have all been seen as materials for green synthesis (Rauwel *et al.,* 2019). Past research findings have reported that incorporating green synthesis into photocatalyst preparation stages often increases the surface area of the photocatalyst, which in turn leads to increased percentage degradation of various organic pollutants.

Aminuzzaman (2017) conducted green synthesis of ZnO nanoparticles. In his research, dragon fruit was obtained, crushed and boiled with distilled water to obtain the extract. The fruit extract was then used as the solvent for synthesis of ZnO from $Zn(NO_3)_2.6H_2O$. The ZnO produced was then characterized with XRD, FT-IR, FESEM, TEM, EDX, XPS, UV-Vis and Raman Spectroscopy. It was observed that ZnO nanoparticles synthesized via green synthesis had better properties than ZnO nanoparticles prepared without green synthesis. It was then suggested that green synthesis method be incorporated for synthesis of photocatalyst**.**

Kaliraj (2019) conducted green synthesis of ZnO for the degradation of dye by UV illumination. In their research, liquid extract from panos leaf was obtained and used as solvent for the synthesis of zinc oxide nanoparticles (ZnONPs) via wet precipitation method. ZnONPs were the characterized with analytical techniques like XRD, FT-IR and FE-TEM. Photocatalytic activity of ZnONPs then conducted on 15 mg/L of methylene blue (MB), Eosin Y (EY) and Malachite green (MG). It was observed that the percentage degradation for each dye was >99%. Reusability studies on ZnONPs was also conducted and no significant decrease in degradation efficiency was observed after five cycles**.**
Osuntokun (2019) also reported the synthesis of photocatalyst (ZnONPs) with extract from broccoli leaf and a percentage degradation of 74 and 71% for MB and phenol red (PR) respectively under UV light irradiation.

Subbiah (2019) conducted research on the photocatalytic activity of green synthesized Mg/Mn doped (0-4%) ZnO nanoparticles (Mg/Mn-ZnONPs) on MB solution. The crystal structure, topological features and composition, surface morphology and chemical bonding of Mg/Mn-ZnONPs was studied through XRD, EDX, SEM and FT-IR analysis.

Photocatalytic degradation of MB solution with Mg/Mn-ZnONP acting as a photocatalyst resulted to an optimum percentage degradation of 94.1% for the first cycle and percentage degradation of 86.3% after five cycles. The minute decrease in degradation efficiency (9%) showed that Mg/Mn-ZnONP could be deployed in large scale applications for wastewater treatment. It was concluded that Mg/Mn-ZnONP possess a high photocatalytic ability and stability under UV irradiation.

Photocatalytic degradation of Rhdodamine B by ZnONPs synthesized using leaf extract of *Cyanometra ramiflora* was studied by Thivaharan (2019). In his research, leaf extract from *Cyanometra ramiflora* was used as solvent for the synthesis of ZnONPs from zinc acetate. The SEM image confirmed the morphology of ZnONPs to be nanoflowers and EDS signals affirmed the presence of zinc and oxygen. XRD results revealed that ZnONPs had a hexagonal wurtzile crystalline structure with a size of 13.33 nm and BET analysis showed that ZnONPs was mesoporous in nature and had a surface area of 16.27 m^2/g. FT-IR affirmed the presence of zinc and oxygen bonding vibrations at 557, 551 and 433 cm^{-1}. The photocatalytic activity of ZnONPs was studied for the degradation of Rhodamine A and a remarkable degradation efficiency of 98% under UV irradiation was achieved within 200 min. It was concluded that green synthesized ZnONPs had an immense potential of degrading organic toxic dyes in wastewater at industrial level.

Plant components such as roots, leaves, stems, seeds, and fruits have been reportedly used for ZnO synthesis. Below is a summary of the synthesis of ZnO nanoparticles by several plant extracts

Table 2.1: Synthesis of ZnO nanoparticles by several extracts from plant

Extracts	Zinc precursor	Size	Shape
Aloe vera	Zinc sulfate	TEM (8–18), XRD (15)	Hexagonal
Azadirachta indica	Zinc nitrate	18 (XRD)	Spherical
Calotropis gigantean	Zinc acetate	8–12 (XRD)	Spherical
Carica papaya milk	Zinc nitrate	11–26 (XRD)	Nanoflower
Coffee	Zinc acetate	4.6 (XRD)	-
Citrus aurantifolia	Zinc acetate	50–200(FESEM)	Spherical
Corymbia citriodora	Zinc nitrate	120 (TEM), 21 (XRD)	Polyhedron
Euphorbia jatropha	Zinc nitrate	50-200 (TEM)	Hexagonal
Moringa oleifera,	Zinc nitrate	16–31.9 (HRTEM)	Spherical, some rod
Plectranthus	Zinc nitrate	C20–50 (TEM)	Spherical hexagonal
amboinicus	Zinc nitrate	33–73 (TEM)	Spherical, aggregation
Polygala tenuifolia	Zinc nitrate	20–30 (XRD),	Hexagonal, quasipherical
Solanum nigrum		29.79(TEM)	

(Source: Zhu *et al*., 2019)

Additionally, due to its excellent physicochemical characteristics, ZnO photocatalyst is currently trending as viable solution to wastewater treatment remediation. Recently, the research community have proven photocatalysis has the capacity to eliminate pollutants from wastewater. Below is a table showing the photocatalytic application of phyto-enhanced ZnO nanoparticles synthesized used in the degradation of various pollutants.

Table 2.3: Photocatalytic application of phyto-enhanced ZnO nanoparticles synthesized for the removal of various contaminants (Zhu *et al*., 2019; Chemingui *et al*., 2019; Khosravi *et al*., 2019)

Plants extract	Pollutants	Time (min)	Degradation (%)
Corymbia citriodora	Methylene blue	90	84
Citrus paradise	Methylene blue	540	56
Plectranthus amboinicus	Methylene blue	180	92.45
Eucalyptus globulus	Methyl orange	60	97
Artrocarpus heterophyllus	Rose bendel dye	120	80
U. lactuca	Methylene blue	120	90
Laurus Nobilis	Textile dye	60	90
Thymus vulgaris	Chromium	15	83

2.10 Doping Technology

The development of an effective heterogeneous photocatalyst has witnessed renewed interest in recent times. As part of the efforts by researchers to improve the photoactivity of a photocatalyst, doping has been suggested (Lam *et al*., 2012). Semiconductors are generally characterized by energy gap. This gap in energy refers to the permissible energy needed for charging electrons impaled in a quantum state to be dissociated to partake in conduction. In a simple term, bandgap accounts for the energy differential of valence and conduction band. Hence the narrower this difference, the wider the spectral and the better the visible light response (Saadati *et al*., 2016). Doping is a technique that imputes trace impurities which serves as inhibitors to e¡/hC recombination during irradiation. These impurities when incorporated into photocatalyst resulting in improved photo activity

(Lam *et al*., 2012). Doping of ZnO with metal ion has been widely considered. It is considered as a feasible way of enhancing the visible light-reaction of ZnO. Metal dopants in some cases are attributed to the scavenging of generated holes/electrons with improved charge carrier lifetime resulting in the inhibition of possible recombination (Saadati *et al*., 2016). However, reports of reduced photo response with metal dopants have been published. It has also been reported that photoactivity of ZnO doped with metals is largely dependent on few parameters namely; choice of metal ion, synthesis procedure and condition of operation. Moreover, there exists an optimum concentration of dopant, above which a negative photoactivity is expected. It has been reported that metals ions such as Na, Ag, Fe, Cr, V, La, Co, Ta and Sn improved photoactivity, whereas Pt, Cu and Mn had opposite consequences. This varying effect is as a result of the ability of the dopants to trap and hinder electron/hole transfer (Saadati *et al*., 2016). The photocatalytic degradation rate of ZnO doped Sn was studied by Sun *et al*., (2011). It was reported that methylene blue was degraded most by the doped ZnO under sunlight. With doped ZnO, methylene blue degradation was successful after 6 hours with approximately 100% COD and TOC removal after 10 hours. Whereas, pure ZnO had 87%, 48% and 71% degradation, COD and TOC removal respectively after 10 hours.

Recently, non-metals such as carbon (C) and nitrogen (N) have been used as dopants for improving the photoactivity of ZnO photocatalyst under sunlight have been considered. In contrast to metals, non-metal ions are less probable to setup recombination centers making them viable alternatives to increase photoactivity. Amongst these non-metals doped ZnO, carbon doping has been reported as the best. This is as a result of the substitution of carbon into the ZnO matrix which necessitated a shift of the valence band edge to a higher energy level consequently narrowing the bandgap. Liu *et al.*, (2011)

studied under visible light irradiation, the photodegradation of RhB by C-doped ZnO. It was opined that the photocatalyst showed strong response in UV–vis ranges. This the authors suggested that it was as a result of carbon taking the position of oxygen in the catalyst and also the large surface area of the photocatalyst, enabling more active sites for photodegradation of the adsorbed pollutant.

2.10 Effects of Reaction Parameters in Photocatalysis

2.10.1 Concentration of pollutant

Pollutant concentration plays a paramount role in its degradation. If initial organic concentration is high, the tendency at which the organic molecule "binds'' itself to the photocatalyst surface and "closes" the active site that leads to hydroxyl radical production will increase and, hence lessen photocatalytic activities of the photocatalyst (Hameed *et al.,* 2011)

Anju (2012) reported the sonophotocatalysis removal of phenol using Zinc oxide. In the authors' view, the rate of degradation increased initially as the initial concentration increases followed by constant degradation rate at higher concentration. Ye (2015) studied the photoactivity of immobilized ZnO nanosheet in the degradation of phenol. He reported the importance of pollutant concentration in the process performance. The author noted that as concentration was increasing from 10 to 60 mg/L, the removal rate was decreasing and after 240 minutes, only 88.5% removal was achieved with the initial concentration of 10 mg/L. This they concluded was as a result of the high concentration of the pollutant which was greater than the hydroxyl radicals generated in the solution. This was similar to the report of Patil and Raut (2012) and Hameed (2011)

2.10.2 Catalyst loading

Catalyst loading effect in photodegradation of pollutants have been reported. Research has shown that degradations in photocatalysis is marked with a linear relationship between catalyst concentration and initial reaction rate (Akpan and Hameed, 2009; Patil and Raut, 2012; Diya'uddeen et al., 2011). Akpan and Hameed, (2009) claimed that any increase in amount of a photocatalyst results in similar rise in the rate of degradation of pollutants. Diya'uddeen (2011) *reported similar observation in degrading cyanosine with varying TiO_2 dosage between 0.01 and 0.08 g/L. The study shows that greater catalyst concentrations resulted in a tremendous increase of active sites available for adsorption. Conversely, increasing the concentration beyond what is required, will not result in a substantial variation in degradation efficiency. This is because excess catalyst acts as blockage to the photon penetration. Several reviews reported a negative degradation of organic pollutants when catalyst concentration is above certain limit. This is in agreement with reports from (Patil and Raut, 2012, Akpan and Hameed, 2009,* Thennarasu and Sivasamy, *2015).*

Hammed (2011) using ZnO to degrade dye did observe that acid dye degradation will rise as more catalyst are added; this is due to the incremental rise in active sites. However, over loading alternatively will hinder the rate of degradation because the excess catalysts may reduce light penetration as a result of screening effect and therefore decrease the photoactivity of the catalyst in use (Akpan & Hameed, 2009). Consequently, it is paramount to determine optimum catalyst dosage in any photocatalytic reaction.

Khan (2014) studied refinery wastewater degradation using zinc oxide and titanium dioxide. The study revealed that degradation was on a rise till 1.2 g/L TiO_2 dosed, thereafter, the degradation decreased. Interestingly, degradation with ZnO followed a

similar pattern until 0.8 g/L after which there was a decrease. This will graphically give a linear regression which implies that degradation has a direct relationship with catalyst loading. This is in agreement with the report of Patil and Raut, (2012). Scrutinizing their findings among several causes for deviation from linearity at high loading, the obvious presumption is the turbidity emanating from more than enough catalyst particles causing unnecessary cloudiness of the wastewater. It can therefore, be presumed that the absorption of UV light by the photocatalyst particles and surface are restricting the absorption of photons within the photocatalytic reactor Abdollahi *et al.* (2012). 1.2 and 0.8 g/l were respectively the optimum concentration of TiO_2 and ZnO respectively in their investigation; which is by far, less than what was reported by Diya'uddeen (2011) and Ye (2015).

2.10.3 Effect of initial pH

Several scholars have reported that pH affects the surface adsorption ability of pollutants on photocatalyst, which is important for the photocatalytic removal of pollutants (Ye *et al.*, 2015, Meshram *et al.*, 2011, Khan *et al.*, 2014 & Anju *et al.*, 2012, Diya'uddeen *et al.*, 2011, Akpan & Hameed, 2009, Abdollahi *et al.*, 2012)

Ye (2015) observed that under extremely high acidic/alkaline condition, phenol removal was significantly low. Their investigation on the effect of varying initial pH (5 to 9) on phenol removal shows removal of phenol under UV light radiation appeared to favour the neutral solution, while lower photocatalytic degradation was noticed at either alkaline or acidic medium.

In another literature, Anju (2012) reported that the extent of UV-catalyzed removal of organics is observed to be reliant on the solution pH. Furthermore, it was noted that the surface properties of the photocatalyst such as band edge position, surface charge and aggregation size was highly influenced by the solution pH. Observations reveal also that degradation rate of organics is high when more targeted molecules are adsorbed successfully to the catalyst surface. This is largely dependent on the acidic/basic nature of the catalyst surface or modified surface as a result of change in solution pH (Meshram *et al*., 2011, Khan *et al.,* 2014 & Anju *et al.,* 2012).

Researches shows that the pH of solution affects the catalyst surface by protonation or de-protonation process (Khan *et al.,* 2014, Akpan and Hameed, 2009; Diya'uddeen *et al.,* 2011). (Diya'uddeen *et al.,* 2011) described the protonation or de-protonation surface of titania according to the equations (2.9) and (2.10):

$$TiOH + H^+ \rightarrow TiOH^{2+} \quad (2.1)$$

$$TiOH + OH^- \rightarrow TiO^- + H_2O \quad (2.2)$$

In addition, the study shows a similar effect of effluent pH on TiO_2 surface, from which they proposed the creation of three (3) different species to justify the disparities of the behaviour of the catalyst with pH. TiOH, $TiOH^{2+}$ and TiO^- *are the suggested species.* At the amphoteric surface, the reactions (2.11) and (2.12) are established owing to the acid–base equilibria dependent on the reaction medium pH as well as the point-of-zero charge (pHpzc) of the catalyst used.

$$TiOH^{2+} \rightarrow TiOH + H^+ \quad (2.3)$$

$$TiOH \rightarrow TiO^- + H \quad (2.4)$$

The equations are a perfect match with those reported by (Akpan and Hameed, 2009)

Meshram (2011) studied the degradation of phenol in a continuous flow photocatalytic reactor using ZnO–bentonite nanocomposite as photocatalyst. They observed that adsorption capacity of organic reactant on photocatalyst is a vital factor when it comes to degradation rate in photocatalytic oxidation process. The study also revealed possible reasons for the successful degradation of phenol attributed to basic medium over acidic medium. Their observations were attributed to two phenomena:

i. Under acidic state – protonation of the active sites which resulted in high adsorption of phenol was due to the charge on ZnO and clay. However, this resulted in a negative outcome as it hindered removal (<5% at pH 2 after 10 min).
ii. Two changes influenced by high pH occur concurrently with phenol and the nanocomposite with clay taking up an alkaline nature and consequently increasing the adsorption capacity whereas the nano-sized ZnO experiences surface modification leading to negatively charged species formation. The two features are responsible for cooperative action of concurrent adsorption trailed by photo degradation of phenol on the nanocomposite surface. Second, phenol experiences deprotonation in a highly alkaline state which further enhanced the rate of adsorption on the nanocomposite. Hence, after a space of 10 min, nearly 66% of phenol was removed at pH level of 12 which suggests the prevalence of second phenomenon concerning the phenol degradation.

2.11 Characterization of Photocatalyst

Characterization of photocatalyst is the act of studying the crystallinity, morphology, functional groups, surface area and pore volume of the photocatalyst through several analytical and laboratory techniques. These analytical techniques include; X-ray Diffractometry (XRD), X-ray Photoelectron Spectroscopy (XPS), Fourier Transform Infrared Spectroscopy (FT-IR), Scanning Electron Microscope/Energy Dispersive X-ray

(SEM-EDX), Brunner Emmett-Teller (BET), X-ray Fluorescence (XRF), Transmission Electron Microscopy (TEM), etc.

2.11.1 X-ray diffraction characterization technique (XRD)

X-ray powder diffraction plays a vital role in material science and engineering (MSE) and research and development (R & D). It is used to study materials (nanomaterials most especially) and evaluate their crystallinity, evaluate the concentrations of each phase in a multiphase specimen, identify the unit cell metrics, conduct microstructure analysis of polycrystalline materials, etc. The diffraction among peaks in a typical XRD result represents X-ray scattering by electrons in various atoms at different positions in the unit cell.

The diffraction from a crystal is described by the equation known as Bragg's law:

$$D = \frac{0.9\lambda}{ßcoscos\,\theta} \tag{2.5}$$

Where D is the crystalline size in nanometer, λ is the wavelength of light, ß is the full-width half maximum and θ is the diffraction degree of the highest peak.

2.11.2 Fourier transform infrared spectroscopy (FTIR)

Fourier Transform Infrared Spectroscopy (FTIR) is used to identify functional groups in solid and liquid samples (Abu 2010). It is centered on the absorption of IR-radiation in chemical bonds of the solid/liquid particle. The spectra of the sample are often cross-referenced with a table containing various ranges of spectra and their likely functional groups/compounds.

CHAPTER THREE

3.0 MATERIALS AND METHODS

3.1 Reagents

Table 3.1: List of Reagents

Reagent & Materials	Purity (%)	Supplier
Zinc Nitrate	99.0	Sigma Aldrich
Urea	99.0	Sigma Aldrich
Sodium Hydroxide Pellets	97.0	Sigma Aldrich
Hydrochloric Acid	37.0	Sigma Aldrich

3.2 Analytical Equipment

Table 3.2: List of Analytical Equipment

S/N	Equipment	Model	Location
1	XRD	Bruker AxSD8 Cu-K radiation	Themba Laboratory Cape town, South Africa
2	UV-Spec	Shimadzu UV-180	STEP-B, FUT-MINNA, Nigeria
3	SEM/EDS	Zeiss Auriga	University of Western Cape, South Africa
4	FT-IR	FT-IR Spectra machine	University of Ilorin, Nigeria
5	BET	NOVA 2400e	STEP-B, FUT-MINNA, Nigeria

3.3 Methodology

3.3.1 Sourcing of paw-paw & leaf extraction

Fresh paw-paw leaves were locally sourced from Minna Niger State, Nigeria. It was then washed with distil water, dried for seven days and milled to obtain a powder form of it. 50 g of the powdery form of paw-paw leaf was then boiled with 200 ml of deionized

water and the liquid extract was separated and stored in a cool environment with a temperature less than 20 ^{o}C.

3.3.2 Determination of the phyto-constituents of paw-paw leaf extract

3.3.2.1 Determination of total phenols

The Folin-Ciocalteau method was employed in quantifying the total phenolic content. Different concentrations ranging from 0.2-1.0 mg/cm^3 of gallic acid and methanol extract of *paw-paw leaf* extracts were prepared in methanol. Thereafter, 4.5 cm^3 of de-ionized water was added to 0.5 cm^3 of the extract and mixed with 0.5 cm^3 of a ten-fold diluted Folin-Ciocalteau reagent. Five milliliters of 7.5 % sodium carbonate were then added to the tubes with another 2 cm^3 of de-ionized water. The mixture was let still for a duration of 90 min at room condition consequent to the absorbance measurement at 765 nm using shimadzu UV spectrophotometer (UV-1800, 240v). This determination was done in threefold with a positive control of gallic acid. This content was expressed as Gallic Acid Equivalent (GAE).

3.3.2.2 Determination of total flavonoids

Determination of total flavonoid constituents of the *paw-paw leaf* was conducted according to the method reported by Chang *et al.,* (2002). Approximately 0.5 cm^3 of the extract was mixed with 1.5 cm^3 of methanol, 0.1 cm^3 of 1 M sodium acetate and 2.8 cm^3 of de-ionized water and allowed for half an hour. The absorbance measurement was conducted at 415 nm using a double beam Shimadzu UV-visible 1800 spectrophotometer. Calibration curve for Quercetin was prepared as standard. Total flavonoid was estimated using the linear relationship;

$$Y = 1.2766x + 0.0448 \quad (3.1)$$

Where: Y =Absorbance (nm) and X= Concentration (mg/L).

3.3.2.3 Determination of total tannins

According to Chang *et al.,* (2002), approximately 2.0 g of the *paw-paw leaf* extract was measured into a 50 cm^3 beaker after which 20 cm^3 of 50 % methanol was added. The beaker enclosed with foil paper was set up in a water bath at 77-80 °C for 1 hour and thereafter shaken to ensure uniform mixing. The resulting mixture was filtered using the Whatman No.1 filter paper into a volumetric flask of 100 cm^3. 20 cm^3 of de-ionized water, 2.5 cm^3 of Folin-Denis solution and 10 cm^3 of 17 % of Na_2CO_3 were added and mixed properly and left for 20 min. The absorbance measurement was observed at 760 nm using Shemadzu UV- spectrophotometer (UV- 1800, 240v). Calibration curve was prepared using tannic acid as standard. Total tannins were evaluated using the Equation (3.2):

$$Y = 0.5269x + 0.602 \quad (3.2)$$

Where Y= Absorbance (nm) and X = Concentration (mg/L).

3.3.3 Synthesis of pure zinc oxide

Twenty grams of Zinc nitrate heptahydrate was weighed using the electronic weighing balance and was poured into a flat bottom flask containing 30 ml of deionized water and the mixture was then stirred thoroughly at 50 rpm for 60 min. Upon the conclusion of stirring, drops of 4 M of sodium hydroxide (NaOH) was intermittently added to the mixture to precipitate zinc oxide. Deionized water was added to the resulting mixture, it was allowed to settle for 30 minutes and the liquid at the top layer of the flat bottom flask was decanted. The washing process was repeated three times. The mixture containing the precipitate and little volume of liquid was dried in the oven at 100 ^oC for 6 h and the dried solid zinc oxide was crushed using an agate mortar to increase its surface area. The weight of the dried zinc oxide was taken and it was observed to be 10 g. The resulting solid

particles (pure zinc oxide) were calcined at 350 ^{o}C for 2 h in a furnace at the Nanotechnology Laboratory, Step-B Federal University of Technology Minna, Nigeria.

3.3.4 Synthesis of green synthesized zinc oxide

Fifty grams of the powdery form of paw-paw leaf was weighed using an electronic weighing balance, it was soaked in 500 ml of distilled water and then heated at 100 ^{o}C for 60 min. Upon conclusion of the boiling procedure, the mixture was filtered and the liquid extract was obtained.

Twenty grams of Zinc nitrate heptahydrate was weighed using the electronic weighing balance and was poured into a flat bottom flask containing 30ml of deionized water and 30 ml of liquid paw-paw leaf extract and the resulting mixture was then stirred thoroughly at 50rpm for 60min. Upon the conclusion of stirring, drops of 4 M of sodium hydroxide (NaOH) was intermittently added to the mixture to precipitate zinc oxide.

Thirty milliliters of deionized water was added to the resulting mixture, it was allowed to settle for 30 minutes and the liquid at the top layer of the flat bottom flask was decanted. The washing process was repeated three times. The mixture containing the precipitate and minute amount of liquid was dried in the oven at 100 ^{o}C for 6 h and the dried solid zinc oxide was crushed using an agate mortar to increase its surface area. The weight of the dried zinc oxide was taken and observed to be 10 g. The solid particles (green synthesized zinc oxide) were calcined at 350 ^{o}C for 2 h in a furnace.

3.3.5 Doping of green synthesized zinc oxide with urea

Ten grams of G.S ZnO and 1g of urea were separately measured and poured into a round bottom flask containing 30 ml of deionized water. The mixture was stirred vigorously at 80 rpm for 6 h and allowed to settle for 30 min. The liquid at the top layer was decanted and the mixture (thick slurry) lower layer in the flat bottom flask was dried in the oven at 100 ^{o}C for 6 h. The resulting solid particles (green synthesized nitrogen doped zinc

oxide) were calcined at 350 ^{o}C for 2 h in a furnace. The process was repeated with 0.2 g and 2 g of urea.

3.3.6 Preliminary studies on degradation of methylene blue solution

The preliminary degradation of Methylene blue solution was carried out using various processes and the following parameters were kept constant; pH of the solution, initial concentration of Methylene blue solution (20 mg/L), catalyst dosage (0.5 g/L) and time (150 min).

3.3.7 Preparation of methylene blue dye solution calibration curve

The calibration curve on the ultra-violet spectrophotometer (UV-Vis Spec) was obtained by preparing various concentrations (20, 40, 60, 80 and 100 mg/L) of Methylene blue solutions and a wavelength of 663 nm was used to calibrate the solution on the UV-Vis Spectrophotometer.

3.3.8 Photolysis on methylene blue dye solution

One hundred milliliters of MB solution with a concentration of 20 mg/L was measured and transferred into a round bottom flask. The solution was then exposed to visible light for 60 min. The concentration of the solution was measured hereafter using the UV-Spec.

3.3.9 Adsorption on methylene blue dye solution

Adsorption experiment was conducted with 0.05 g of the 5 % green synthesized nitrogen doped zinc oxide (5% G.S N-ZnO) photocatalyst. The sample was weighed on an electric weighing balance and transferred into a flat bottom flask containing 100 ml of 20 mg/L of Methylene blue solution. The solution medium (flat bottom flask) was then transferred into a cupboard and the solution was stirred at 50 rpm with a magnetic stirrer for 60 min. 10 ml of the solution was taken from the solution and allowed to settle 10 min so as to separate the photocatalyst. The concentration of the clear liquid sample solution after decantation was measured using the UV-Spec.

3.3.10 Photodegradation of methylene blue dye

Photodegradation of MB was conducted with pure and green synthesized zinc oxide. The experiment started by measuring of 0.05 g pure zinc oxide on a weighing balance. The weighed sample was then transferred into a flat bottom flask containing 100 ml of 20 mg/L of Methylene blue solution. The solution was first stirred in the absence of visible light at 50 rpm for 30 min and this was done to ensure absorption-desorption equilibrium was attained before the photocatalytic reaction. The flat bottom flask containing the reactants was then exposed to visible light for 150 min with continuous stirring at 50 rpm. 10 ml of the solution was taken from the solution and allowed to settle for 20 minutes. Decantation was then performed to separate the clear liquid at the upper later. The concentration of the clear liquid was then measured with the UV-Spec and recorded. Similar procedures were repeated for 5 % and 10 % green synthesized nitrogen doped zinc oxide.

3.3.11 Effects of solution pH, time & initial concentration on percentage degradation

The response of percentage degradation of MB to process parameters were studied. These parameters included; solution pH, catalyst dosage and Initial concentration. The results obtained from preliminary experiments informed the structure of the experiments carried out when studying the effects of pH, catalyst dosage and Initial concentration on percentage degradation.

3.3.12 Characterization of pure ZnO and green synthesized doped

Characterization of pure zinc oxide and green synthesized nitrogen doped zinc oxide were conducted with analytical techniques like XRD, SEM-EDX, BET and FTIR.

3.3.12.1 Experimental conditions for surface electron microscopy

0.05 g each of zinc oxide and green synthesized zinc oxide synthesized samples was sprinkled on a Carbon tape which was fixed onto an aluminum stub. The zinc oxide and

green synthesized zinc oxide synthesized were coated with gold-palladium (Au:Pd; 60:40) using Quorum T15OT for five (5) minutes preceding the analysis. The essence of this, is to prevent charging which interfere with images during analysis. To examine the morphology and elemental makeup of the samples, the Zeiss Auriga SEM couples with EDS were respectively used. The microscope ran at 5 KeV for imaging and 20 KeV detectors for EDS.

3.3.12.2 Measurement conditions for energy dispersive x-ray (EDX)

0.05 g each of zinc oxide and green synthesized zinc oxide synthesized samples was sprinkled in a sample holder covered with carbon adhesive tape which was sputter-coated with Au-Pd using Quorum T15OT for 5 min to the commencement of analysis. The sputter coated samples were characterized using Zeiss Auriga SEM. The secondary electron mode was activated for imaging and a homogeneous region on the sample was identified. The microscope was operated with electron high tension (EHT) of 20 KV for EDS, the illumination angle was adjusted to 150° and then the elemental composition of the sample was determined.

3.3.12.3 Measurement conditions for x-ray diffraction (XRD)

1 g each of the zinc oxide and green synthesized zinc oxide synthesized samples was crushed into powder and then dispersed into a rectangular aluminum sample holder with the aid of a well cleaned spatula. The sample holder containing the sample was clipped into the XRD instrument. Bruker AXS Advance diffractometer with 2θ range of 5 - 75°, a step size of 0.028°, and operating at 45 KV and 40 mA was used to collect the XRD data. Monochromatic copper (Cu) Kαl radiation with a wavelength of 0.154nm was as the X-ray source. The mean crystallite size of the nanoparticles (D), were obtained using the Debye-Scherrer equation:

$$D = \frac{0.89\lambda}{ßcoscos\,\theta} \qquad (3.3)$$

Where k is a Constant (k=0.89), λ = 1.54060 nm is the Cu- Kαl wavelength, θ is the Bragg's angle and β is the full width half maximum (FWHM) of the peak at 2θ (Kaur *et al*., 2019).

3.3.12.4 Experimental conditions for Brunner-Emmett-Teller (BET)

The analysis for the surface area, pore volume and pore size distribution of the sample was determined by Brunauer - Emmett- Teller (N_2 BET) technique using a NOVA 4200e surface area and pore analyzer instrument. 100 mg each of the zinc oxide and green synthesized zinc oxide synthesized photocatalyst powder was weighed and degassed by flowing N_2 at 90 °C for 1 hour, and then held at 350 °C for 2 hours. As the temperature is increased, water vapour was adsorbed from the surface and pores of the sample. The sample was left to cool down and weighed again. The instrument uses physical adsorption and capillary condensation of N_2 principles to abstain information about the surface area and porosity of ZnO.

CHAPTER FOUR

4.0 RESULTS AND DISCUSSION

4.1 Phytochemical analysis of Paw-paw Leaf Extract

Table 4.1 shows quantitative results obtained after phytochemical screening was conducted on extract of the *Paw-paw* leaf.

Table 4.1 Phytochemical Assessment of the *Paw-paw* Leaves Extract

Contents	Concentration (mg/100g)
Phenol	447.64
Flavonoid	47.96
Tannins	14.99
Alkaloids	26.47
Saponins	164.22

The phytochemical assessment was conducted to determine the phytochemicals present in Paw-paw leaf extract. It was observed that phenol, flavonoids, tannins, alkaloids and saponin were present in significant amounts. These phytochemicals are responsible for the capping and stabilization of nanomaterials. This implies that these plant extracts behave in a similar manner with the commercial reducing agents such as citric acid, sodium borohydride ($NaBH_4$), lithium aluminium hydride ($LiAlH_4$).

4.2 Preliminary studies

Table 4.2: Preliminary results for degradation of methylene blue dye

S/N	Process	C_o (mg/L)	Time (min)	Degradation (%)
1	Pure ZnO	20	150	53.45
2	GS ZnO	20	150	56.25
3	2% GS N-ZnO	20	150	60
4	5% GS N-ZnO	20	150	72.6
5	10% GS N-ZnO	20	150	68.3

Table 4.2 presents the results of preliminary studies conducted for the degradation of methylene blue (MB) at an initial concentration of 20 mg/L for 150 min. Photolysis was observed to degrade 8.5 % of the MB pollutant. This affirms that photolysis is ineffective for complete degradation of MB in municipal and industrial wastewater containing dye pollutants. Also, 26.72 % of MB was degraded when adsorption process was employed and this was deemed to be low too even though it was an improvement from Photolysis. Further studies with pure ZnO and various samples of G.S N-doped ZnO revealed that 5 % G.S N-doped ZnO had superior performance compared to its counterparts. It was adopted for the remaining experiments where effects of solution pH, catalyst dosage and initial concentration of MB solution on percentage degradation were studied.

4.3 Characterization of Nitrogen Doped Zinc oxide

4.3.1 Fourier transform infrared spectroscopy analysis

The synthesized ZnO and doped ZnONPs were characterized by FTIR technique and are presented on Figure 4.1.

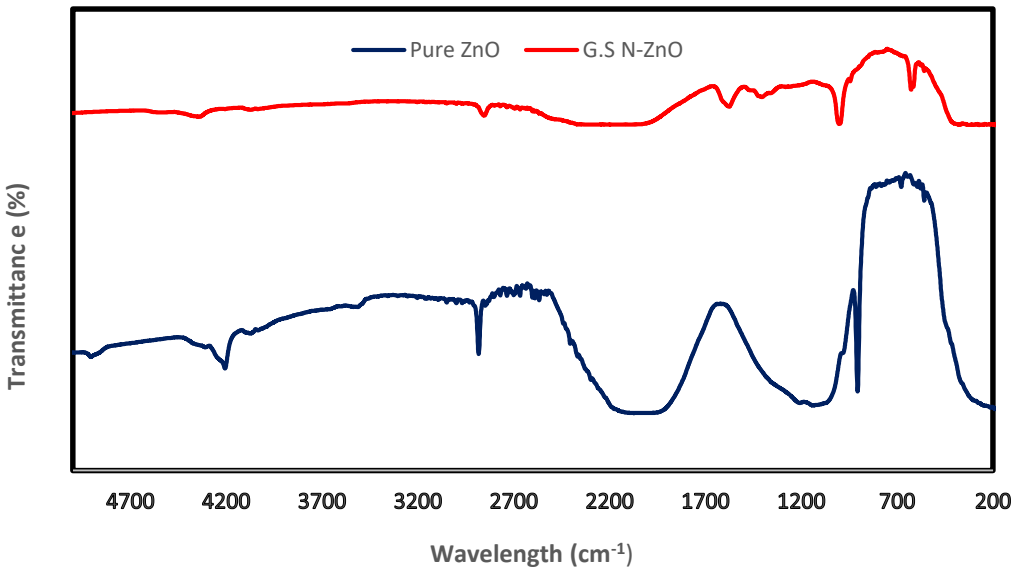

Figure 4.1: *FTIR* spectra for pure ZnO and green synthesized doped ZnO nanoparticles

The FTIR spectra revealed functional groups in all the samples investigated. These functional groups were observed in the scan range of 4000–500 cm^{-1}. The characteristic peak in X of Figure 4.1 at 3484.68 cm^{-1} belongs to the O-H group whereas 2764.87cm^{-1} represents C-H_3 stretching in amines, while 2426.52 cm^{-1} shows the presence of N-D stretching in Amines. In addition 1788.45 cm^{-1} corresponds to C-O of aliphatic diacyl peroxide. The peak at peak 1402.79 cm^{-1} corresponds to C-H deformation of Cycloalkanes. The peak at 1342.61 corresponds to the C-H deformation of acetates, the

peak at 946.74 corresponds to the C-H out-of-plane deformation of Vinyl halogen compounds and the peak at 834.27 reveals the presence of P-CH_3. Similarly, the FTIR spectrum for the nitrogen doped ZnO {Figure 4.1 (Y)} showed several peaks. The introduction of Nitrogen from Urea (CH_4 N_2 O) as dopant led to some modifications during the synthesis of the photocatalyst. The peaks between 1500 – 600 cm^{-1} shows the typical fingerprint region of ZnO nps. The peaks at 1670.13, 1653.58, 1647.16, 1636.12 cm^{-1} revealed the N-H bonding and affirmed the presence of $–NH_2$ from Urea.

4.3.2 Scanning electron microscope analysis

Scanning electron microscope (SEM) has been reported to be one of the notable leading techniques for the determination of the topo-graph of prepared samples. It is known for providing vital facts about the morphological shape of synthesized samples. The SEM micrograph (Plate II) at different magnifications confirmed that ZnO nanoparticles were formed.

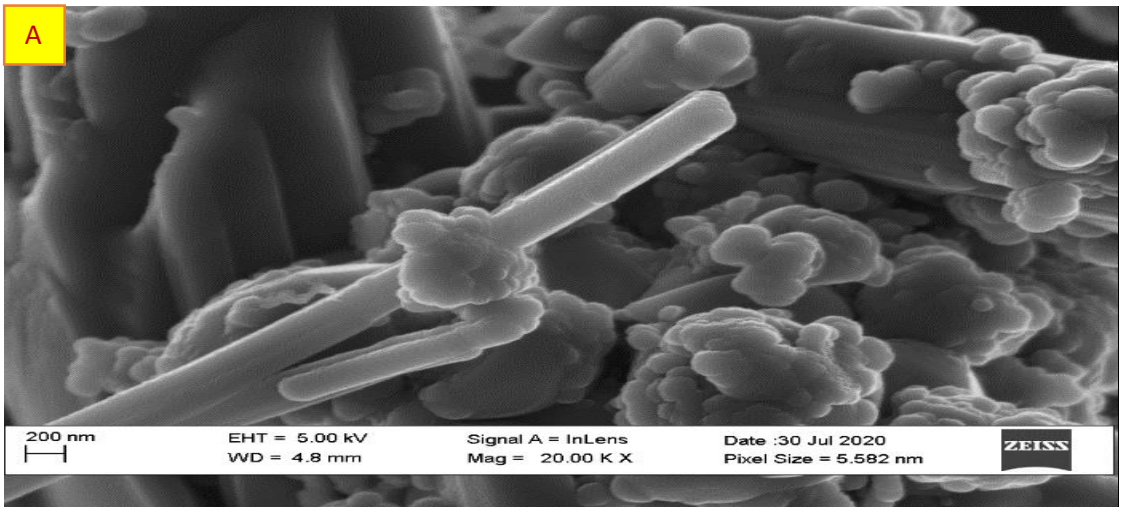

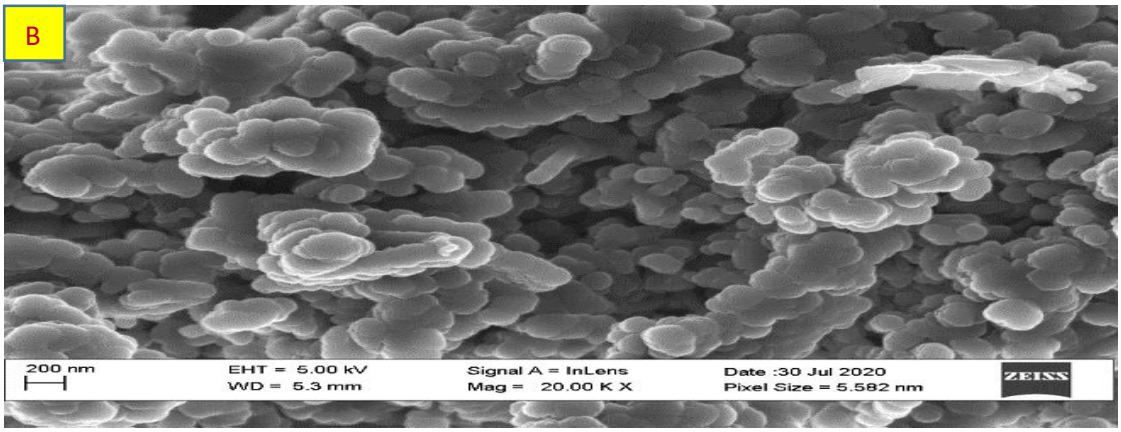

Plate II: SEM micrograph of pure ZnO (A) and G.S N-doped ZnO (B)

The SEM image for synthesized pure zinc oxide (ZnO) reveals a network configuration of an agglomerated blend of elongated rod-like shapes and selfsame spheres. Whereas, the SEM micrograph of the doped zinc oxide nanoparticles reveals loosed structure of uniformly distributed particles with increased surface area. The nanoparticles were spherical and granular in nature. In addition, the nanoparticles were aggregated due to the surface-to-volume ratio which is typical with nanoparticles as suggested in many literatures (Balogun *et al*., 2020). This is because nanoparticles are known for their large surface area with notable inclination for attraction between particles (Barziny *et al.*, 2020).

4.3.3 Energy dispersive x-ray

The elemental composition of pure ZnO and that of modified ZnO nanoparticles with their respective atomic and weight percent were verified by energy dispersive spectrum (EDS) analysis as shown in Figure 4.2. The observed spectra of the samples in Figure 4.2, shows that it contained traces of impurities as a result of the container used to hold the samples.

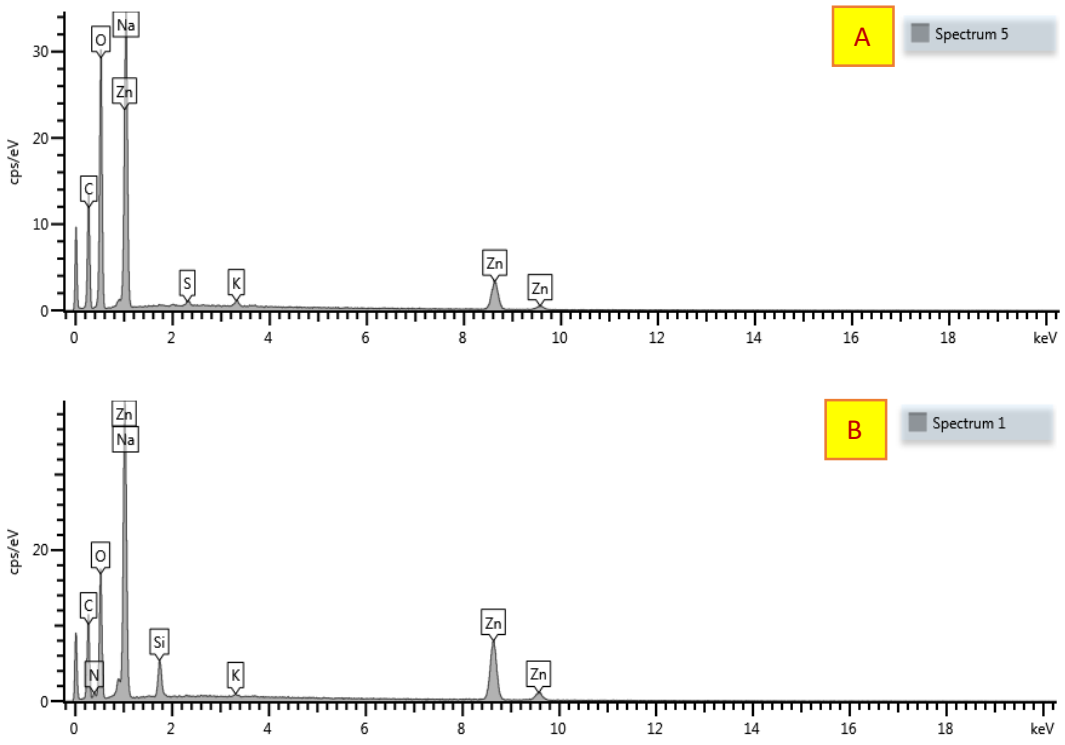

Figure 4.2**:** EDX of pure ZnO and GS N-doped ZnO nanoparticles

The peak of Zinc (Zn), Oxygen (O), carbon(C), Sodium (Na), potassium (K) and Sulphur(S) were all observed for the synthesized pure zinc oxide (ZnO). However it was observed that peaks of Zinc (Zn), Oxygen (O), Carbon(C), Sodium (Na), Magnesium (Mg), Phosphorous (P) and Potassium (K) were present in the green synthesized doped ZnO nanoparticle. The EDX spectra of pure ZnO revealed three peaks for Zinc (Zn) at 0.4, 4.2, and 24.0 keV as against the EDX spectra of green synthesized doped ZnO which revealed peaks for Zinc (Zn) at a 1.0, 8.6, and 29.0 keV. The difference in peaks for Zinc (Zn) and other elements in both spectra and the presence of Nitrogen in the EDX spectra of Nitrogen doped Zinc oxide affirms the modification of ZnO nanoparticles which improved after green synthesis and doping process (Barziny, 2020). The observed peaks of Potassium (K), Sulphur(S), magnesium (Mg) and phosphorus (P) in traces could be attributed to surface contamination during the analysis. In addition, the carbon peaks

observed may be attributed to the carbon composition of the storage material and the carbon introduced by the dopant.

4.3.4 X-ray diffraction analysis

Powder XRD analysis was conducted to identify the phase composition, lattice parameter and crystalline size of the pure ZnO and N-doped ZnO. The XRD pattern clearly indicates crystalline structure for pure and doped ZnO nanoparticles. The 2θ values for Pure ZnO corresponded to diffraction peaks were 31.80, 34.28, 36.17 47.59, 56.62, 62.92, 66.41, 68.00, 69.13^{o} and for pure ZnO nanoparticles, 2θ values were 31.80, 34.48, 36.29, 47.58, 56.62, 62.92, 68.00, 69.13 degrees for doped ZnO.

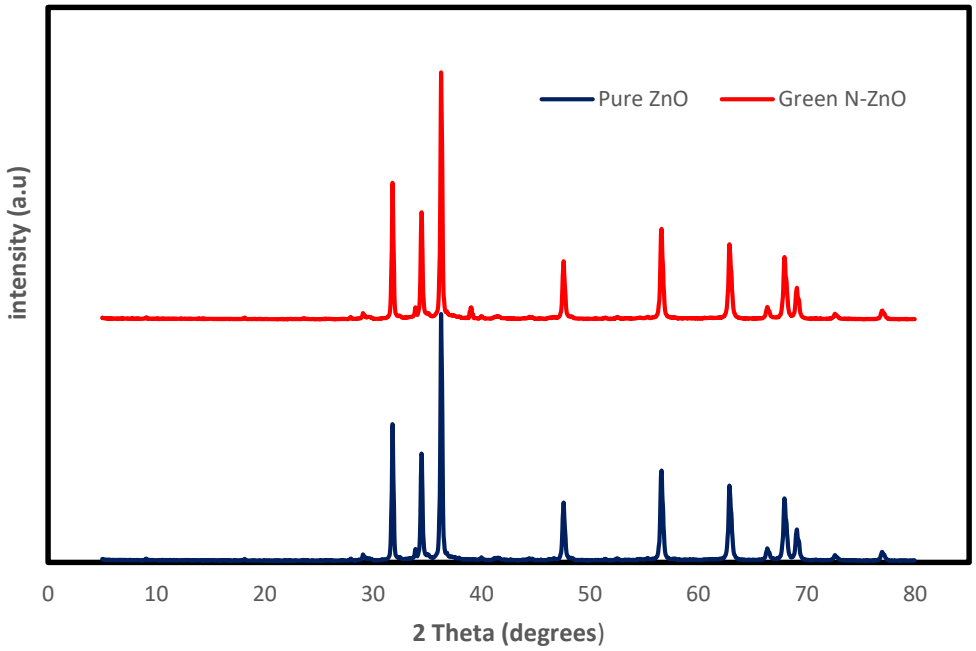

Figure 4.3: XRD spectrum for ZnO and green synthesized nitrogen-doped ZnO

These peaks correspond to the miller index (100), (002), (101), (102), (110), (103) and (112) in that order. This affirmed that the N-doped ZnO has a hexagonal wurtzite structure (Prabakaran *et al*., 2019) which was in good agreement with JCPDS card no 36-1451. The crystalline size of Nitrogen doped ZnO nanoparticles was calculated with the Bragg's formula as shown in Equation 4.1:

$$D = \frac{0.89\lambda}{ß cos\theta} \quad (4.1)$$

Where D is the crystallite size of N-doped ZnO photocatalyst, λ is the wavelength of the X-ray beam operating system, ß is full width half maximum and θ is the angle of diffraction. The crystallite size of pure ZnO nanoparticles was calculated as 18nm and the size of doped ZnO photocatalyst was calculated as 8.435nm. This decrease in crystallite size in nitrogen-doped doped ZnO catalyst as compared to ZnO confirmed an increase in surface area for the former and also a better performance by the former during Photocatalysis.

4.3.5 BET analysis

The surface area and pore size of Nitrogen doped ZnO nanoparticles catalyst was investigated through the BET method under nitrogen gas Adsorption processes as shown in Table 4.3. The surface area and pore size/diameter of phyto enhanced doped ZnO were obtained to be 113.3 m^2/g and 2.118nm respectively, whereas, that of pure ZnO were obtained to be 22.27m^2/g and 1.453nm respectively. The increase in surface area and pore size on phyto enhanced doped ZnO compared with pure ZnO further confirmed the photocatalytic degradation potential of nitrogen-doped ZnO.

Table 4.3: BET Summary

Photocatalyst	Surface area (m^2/g)	Pore diameter(nm)	Pore volume(cm^3/g)
Pure Z_nO	22.27	1.453	0.010
G.S Doped N-Z_nO	113.3	2.118	0.055

4.4 Effect of operating parameters on the degradation of methylene blue dye

4.4.1 Effect of photocatalyst dosage on the degradation of methylene blue dye

In the past few years, various research studies related to Photocatalysis has reported that photocatalyst dosage/loading influenced the rate of degradation of organic pollutants. In this study, the influence of different amounts of doped nitrogen zinc oxide (N-ZnO) nanoparticles on the rate of degradation of methylene blue dye was investigated. As seen on Figure 4.4 below, it is observed that an increase in amounts of N-doped ZnO photocatalyst led to a corresponding increase in percentage degradation until the catalyst dosage exceeded 100mg, where percentage degradation began to decrease. The decline of percentage degradation after photocatalyst dosage exceeded 100 mg can be attributed to the decrease in visible light penetration on the photocatalyst which occurred due to aggregation of the photocatalyst and increase in turbidity of the solution. It can therefore be established that the amount of doped ZnO nanoparticles required for optimum degradation of methylene blue dye solution is 100 mg.

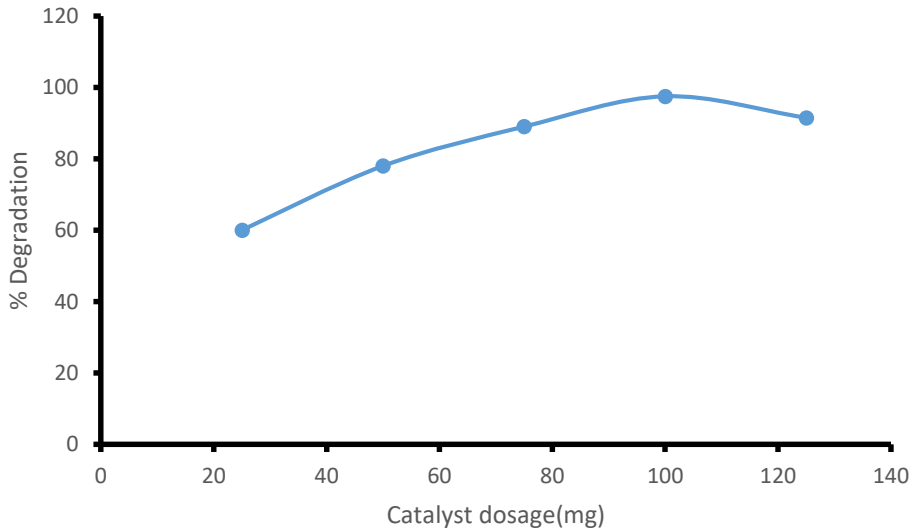

Figure 4.4: Effect of photocatalyst loading on degradation of MB

4.4.2 Effect of solution pH

The pH of the solution controls the mode of adsorption of the targeted molecules and its subsequent photocatalytic degradation by influencing the ionization state visa-viz the electrical charge characteristics of the surface of the photocatalyst. The pH of the solution was adjusted with sodium hydroxide (NaOH) and hydrochloric acid (HCl). From Figure 4.5, it is observed that low percentage degradation of methylene blue (MB) was recorded when pH of the solution was below six, the highest percentage degradation of MB was recorded at pH 9 and the percentage degradation of MB began to decline after the pH of the solution exceeded 9. This phenomenon can be linked to the behavior of MB at different pH and the surface-charge properties of the photocatalyst explained by point zero charge. At pH < 6.0, MB exists in a cationic form, at pH = 6.0 ~ 7.7 as zwitterion and at pH > 7.7, MB exists as anion. In addition, the point zero charge of the photocatalyst (N-doped ZnO) is estimated to be 9.3. Therefore, at a pH<6, MB solution exists as a cation and tends to repel from the surface of the photocatalyst existing as a cation. This results in low adsorption which leads to low percentage degradation. However at a pH > 7.7, MB solution exists as an anion and is drawn to the surface of the photocatalyst by strong electrostatic forces. This then leads to more adsorption on the surface of the photocatalyst and thereafter higher rate of degradation. The decline in the rate of degradation after pH of the solution exceeded 9.0 can be attributed to the occurrence of repulsion occurring between the MB anions and the surface of the photocatalyst which is negatively charged above a pH of 9.0. It can therefore be established that pH of 9 is the optimum pH required to obtain the highest degradation of MB dye with green synthesized N-ZnO acting as photocatalyst.

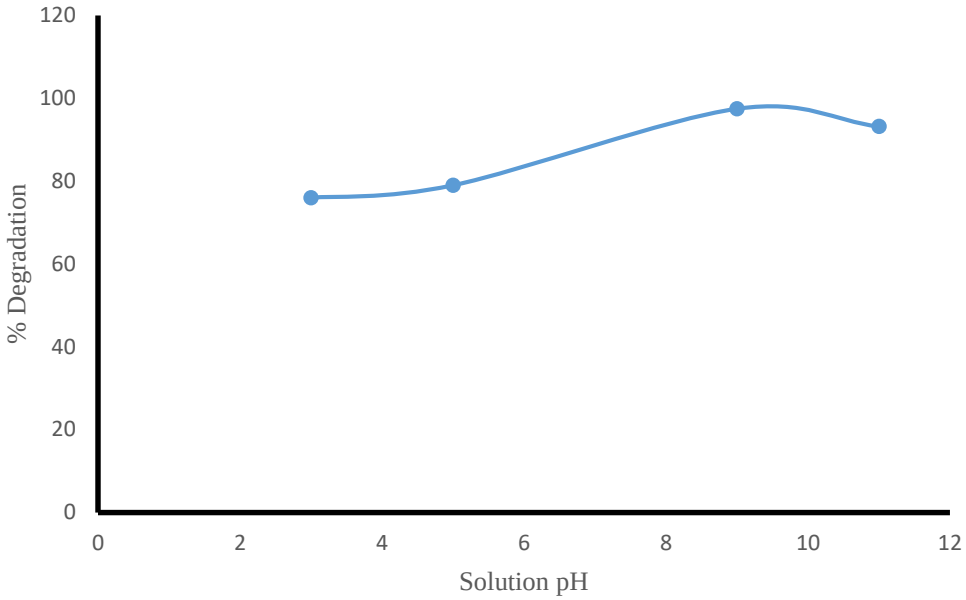

Figure 4.5: Effect of solution pH on degradation of MB

4.4.3 Effect of initial concentration of methylene blue dye

The initial concentration of methylene blue dye solution is also a key parameter that influences the rate of degradation of MB during Photocatalysis.

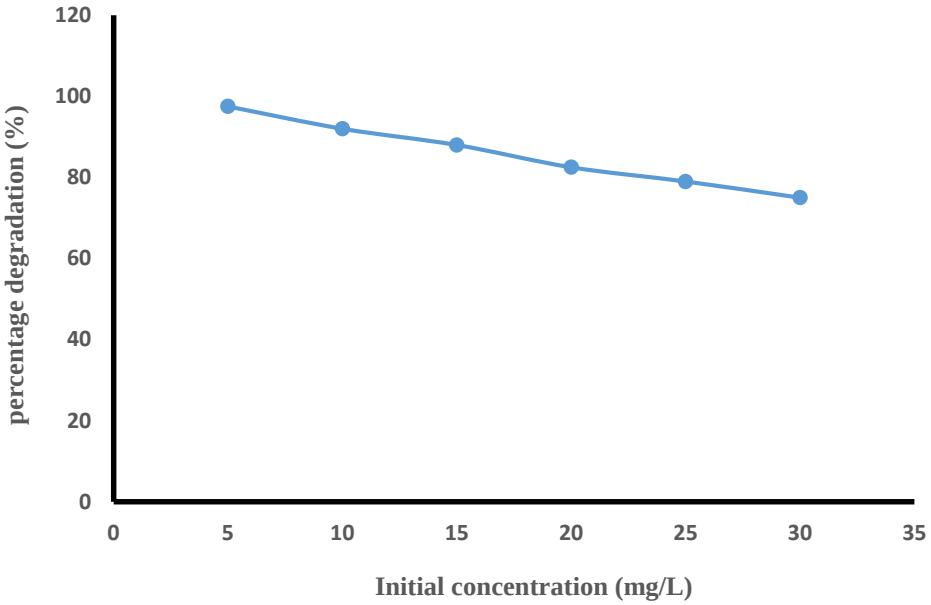

Figure 4.6: Effect of initial concentration on degradation of MB

From Figure 4.6, it is observed that percentage degradation decreased as initial concentration of methylene blue dye solution increased. This phenomenon can be attributed to the decrease in light penetration on the surface and active sites of the photocatalyst.

4.4.4 Reaction kinetics

Reaction kinetics study was conducted for the photocatalytic process and was observed to follow the first order kinetics. Figure 4.7 reveals a linear relationship between ln (C_o/C_t) and time and this affirmed the occurrence of the first order kinetics; ln (C_o/C_t) = K_c t. Where C_o & C_t are initial and final concentration respectively, K_c = rate constant, t = time in minutes. The slope of each linear plot on figure 4.7 represents the rate constants (K_c) for the first order photocatalytic reactions. The K_c values for 5, 10, 15 and 20 mg/L initial concentrations were 0.0477 min^{-1}, 0.0345 min^{-1}, 0.0278 min^{-1} and 0.0246in^{-1} respectively.

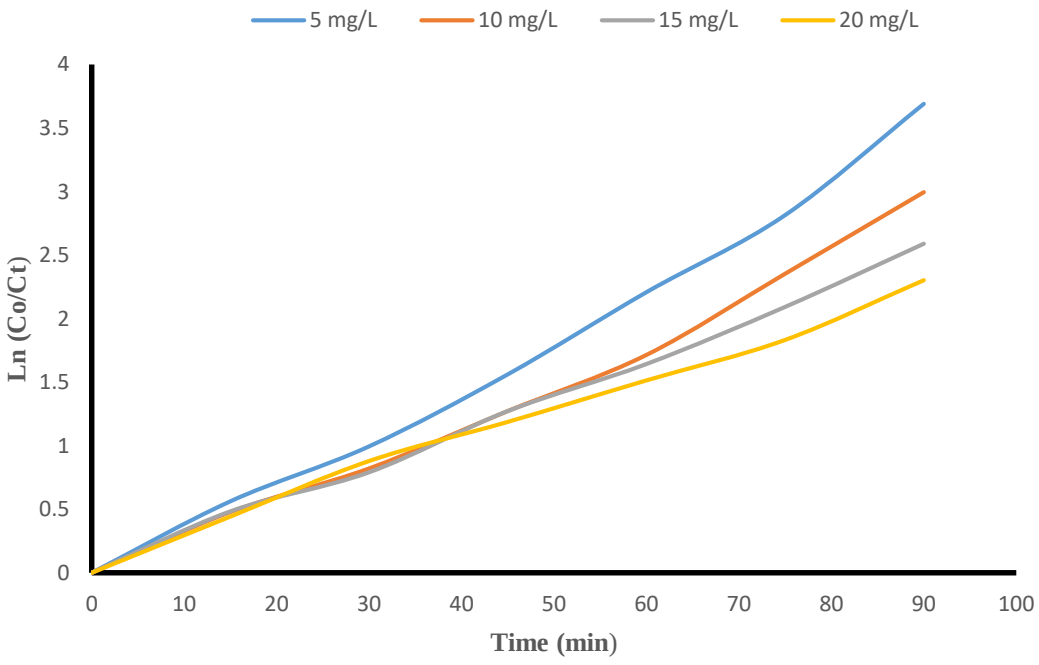

Figure 4.7: Plot of ln (C_o/C_t) vs time

Table 4.4 Kinetic parameters for photocatalytic degradation of methylene blue dye

Concentration (mg/L)	Linear Equation	Rate constant (k)
5	y = 0.0477x – 0.2366	0.0477
10	y = 0.0298x - 0.1855	0.0345
15	y = 0.0278x - 0.0993	0.0278
20	y = 0.0204x - 0.141	0.0264

4.4.5 Proposed reaction mechanism

The following reactions represent the proposed reaction mechanism for the photocatalytic degradation of the methylene blue dye with green synthesized nitrogen doped zinc oxide.

1. Absorption of efficient photons ($h\nu \geq E_G$ = 3.2 eV) by green synthesized nitrogen doped zinc oxide

$$\text{N-ZnO (photocatalyst)} + h\nu \longrightarrow e^-_{CB} + h^+_{VB} \quad (4.2)$$

2. Oxygen ion-sorption (oxygen's oxidation degree passes from 0 to −1/2)

$$(O_2)\ \text{ads} + e^-_{CB} \longrightarrow O_2^{o-} \quad (4.3)$$

3. Neutralization of OH^- groups by photo-holes which produces OH° radicals

$$(H_2O \Leftrightarrow H^+ + OH^-)\ \text{ads} + h^+_{VB} \longrightarrow H^+ + OH^\circ \quad (4.4)$$

4. Neutralization of O_2^{o-} by protons

$$O_2^{o-} + H^+ \longrightarrow HO_2^{o-} \quad (4.5)$$

5. Transient hydrogen peroxide formation and dismutation of oxygen

$$2HO_2^{o-} \longrightarrow H_2O_2 + O_2 \quad (4.6)$$

(hydro peroxide)

6. Decomposition of H_2O_2 and second reduction of oxygen

$$H_2O_2 + e^- \longrightarrow OH^\circ + OH^- \quad (4.7)$$

7. Oxidation of the organic reactant via successive attacks by OH° radicals

$$R + OH^\circ \longrightarrow R^\bullet + H_2O \quad (4.8)$$

8. Direct oxidation by reaction with holes

$$R + h^+ \rightarrow R^{+\circ} \longrightarrow \text{degradation products} \quad (4.9)$$

(akyl group)

9. As an example of the last process, holes can react directly with carboxylic acids

$$RCOO^- + h^+ \longrightarrow R^\bullet + CO_2 \quad (4.10)$$

10. Expected overall reaction

$$C_{16}H_{18}N_3S + OH^\circ \longrightarrow CO_2 + H_2O \quad (4.11)$$

(methylene blue)

From the series of reactions presented above, the major rate limiting step is the first equation where initiation of the reaction occurs. This is because adequate amount of visible light with bandgap energy higher than of the photocatalyst is required to excite electrons from the valence band to the conduction band of the photocatalyst. The excited electrons reduces dissolved and atmospheric oxygen to superoxide radicals which a key to the degradation of organic pollutants.

4.4.6 Data fitting and comparison between experimental and estimated data

The estimated concentration (Ca) for the 1^{ST} and 2^{ND} order kinetic equations were computed with the Scipy Library of Python Programming software. The rate constant (k) for 1^{ST} and 2^{ND} kinetics was calculated using the minimize function of the Scipy.optimize

module and then the numerical values of rate constant obtained for each kinetic was obtained.

A plot of Ca against time for experimental and estimated data (Ca) was then produced, and it was observed that 1ST order kinetics had better fittings than that of 2ND order kinetics. This supports the photocatalytic reaction was a first order reaction. The data fittings for the 1ST and 2ND order kinetics are presented in Figure 4.8.

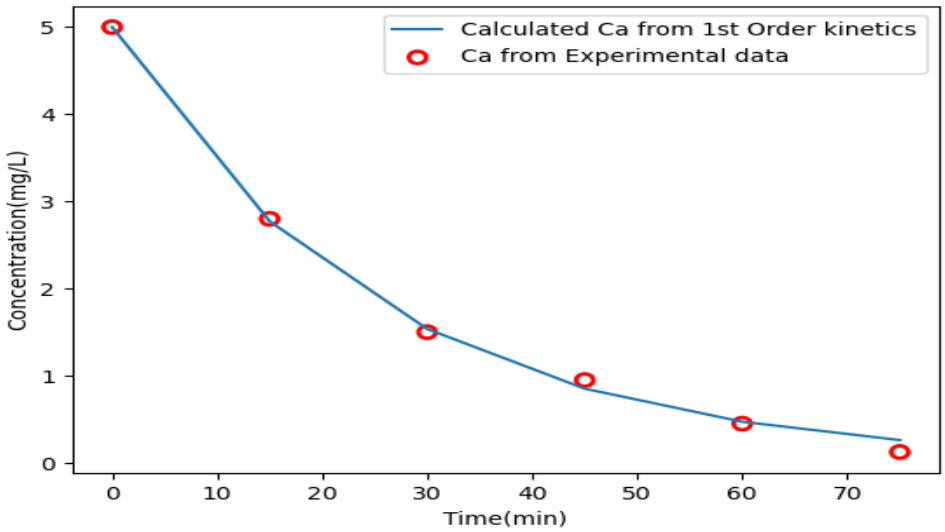

(a)

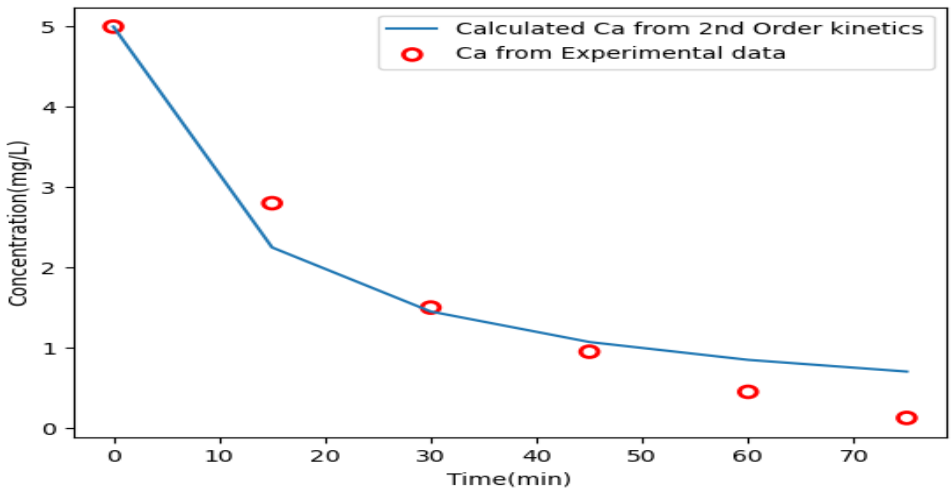

Figure 4.8 a and b: Estimated and Experimental Ca for 1^{ST} and 2^{ND} order kinetics

4.4.7 Sum of square error (SSE) analysis

The sum of square error (SSE) analysis was computed with the value of k for 5 mg/L initial concentration from Table 4.4

The Scipy Library of Python Programming language was used to conduct error analysis and the code below presents the lines of code for the error analysis.

```
import numpy as np
from scipy.optimize import minimize

Cao = 5.0
c = np.array([5,3.75,3.09,2.48,1.59,0.12])
t = np.array([0,15,30,45,60,75])

def kine(k,t,c):
    c_cal = np.zeros(len(c))
    for i in range(0,len(c)):
        c_cal[i] = Cao - (np.exp(k*t[i]))
    res = c_cal - c
    SSE = sum(res**2)
    return SSE

OPM = minimize(kine,0.0477,args=(t,c))
k = OPM.x

#reevaluation of parameters
c_cal = np.zeros(len(c))
for i in range(0,len(c)):
    c_cal[i] = Cao-(np.exp(k*t[i]))

res = c_cal - c
SSE = sum(res**2)

print(res)
print(res**2)
print(SSE)
```

Where cal_c = estimated Ca, c = experimental Ca, t = time, SSE = sum of square errors and Cao = Initial concentration

Table 4.5: Sum of Square Error (SSE) analysis

S/N	Time (min)	Experimental Ca	Estimated Ca	Error (E)	Square errors (SE)
1	15	3.75	3.6394	-0.1188	0.0141213
2	30	3.09	3.1488	-0.0363	0.0013174
3	45	2.48	2.4813	-0.0448	0.00200596
4	60	1.59	1.5731	-0.1008	0.01015388
5	75	0.12	0.3375	0.0743	0.00552745
					Σ of SE = ~ 1.0331

CHAPTER FIVE

5.0 CONCLUSION AND RECOMMENDATIONS

5.1 Conclusion

i. Green synthesized zinc oxide nanoparticles was synthesized from an aqueous solution of Zinc nitrate hexahydrate and *Papaya leaf* extract, and doped with nitrogen from Urea

ii. Pure zinc oxide and green synthesized nitrogen doped zinc oxide were characterized with SEM-EDX, FTIR, XRD and BET analyses and the results revealed a distinct difference between both solid samples (pure zinc oxide and green synthesized nitrogen doped zinc oxide).

iii. The highest percentage degradation of methylene blue dye with pure zinc oxide and green synthesized nitrogen doped zinc oxide as photocatalysts were 83% and 97.5% respectively and these were observed to occur at solution pH of 9.0, photocatalyst dosage of 100 mg and Initial concentration of 5 mg/L.

iv. This study has demonstrated that photocatalytic degradation of methylene blue dye could be improved by incorporating green synthesis and doping during the photocatalyst preparation. It has also revealed that synthesis of nanoparticles could be made less-hazardous and eco-friendly.

5.2 Recommendations

Effects of sunlight intensity on Photocatalysis should be further explored. In addition, the reaction mechanism should be studied with high performance liquid chromatography (HP-LC) and gas chromatography mass spectrometry (GC-MS).

5.3 Contribution to Knowledge

In this research, physicochemical properties of Zinc oxide (ZnO) enhanced with doping and green synthesis. This resulted to 98% degradation of methylene blue dye which was greater than 80% degradation of MBD when pure Zinc oxide was used.

REFERENCES

Adhikari, R., Gyawali, G., Cho, S. H., Narro-García, R., Sekino, T., & Lee, S. W. (2014). Er3+/Yb3+ co-doped bismuth molybdate nanosheets up conversion photocatalyst with enhanced photocatalytic activity. *Journal of Solid State Chemistry*, *209*, 74-81.

Ahmadi, M., Motlagh, H. R., Jaafarzadeh, N., Mostoufi, A., Saeedi, R., Barzegar, G., & Jorfi, S. (2017). Enhanced photocatalytic degradation of tetracycline and real pharmaceutical wastewater using MWCNT/TiO2 nano-composite. *Journal of environmental management*, *186*, 55-63.

Aljuboury, D. A. D. A., Palaniandy, P., Abdul Aziz, H. B., & Feroz, S. (2017). Degradation of total organic carbon (TOC) and chemical oxygen demand (COD) in petroleum wastewater by solar photo-Fenton process. *Global NEST Journal*, *19*(3), 430-438.

Akpan, U.G, Hameed, B.H. (2009): Parameters affecting the photocatalytic degradation of dyes using TiO2-based photocatalysts: *A review, Journal of Hazardous Materials* 170 (2009) 520–529

Aminuzzaman, M., Ng, P. S., Goh, W. S., Ogawa, S., & Watanabe, A. (2019). Value-adding to dragon fruit (Hylocereus polyrhizus) peel biowaste: green synthesis of ZnO nanoparticles and their characterization. *Inorganic and Nano-Metal Chemistry*, *49*(11), 401-411.

Amita K, & Rana, P. S. (2019). Visible light photocatalysis of methylene blue using cobalt substituted cubic NiO nanoparticles. *Bulletin of Materials Science*, *42*(4), 1-11.

Ani, I. J., Akpan, U. G., Olutoye, M. A., & Hameed, B. H. (2018). Photocatalytic degradation of pollutants in petroleum refinery wastewater by TiO2-and ZnO based photocatalysts: recent development. *Journal of cleaner production*, *205*, 930-954.

Anirudhan, T. S., & Deepa, J. R. (2017). Nano-zinc oxide incorporated graphene oxide/nanocellulose composite for the adsorption and photo catalytic degradation of ciprofloxacin hydrochloride from aqueous solutions. *Journal of colloid and interface science*, *490*, 343-356.

Anju, S.G (2012) Sono, Photo and Sonophoto Catalytic Removal of Chemical and Bacterial Pollutants from Wastewater, *Thesis submitted to Cochin University of Science and Technology.* Kochi - 682 022

Asman Olthman, D. Jini, M. Aravind, C. Parvathiraja, R. Ali, M. Zaheer Kiyani, A. Ahmad (2020). A Novel study on Synthesis of Egg shell based activated carbon for degradation of methylene Blue via photocatalysis, *Arabian Journal of Chemistry* (2020).

Balogun, S. W., James, O. O., Sanusi, Y. K., & Olayinka, O. H. (2020). Green synthesis and characterization of zinc oxide nanoparticles using bashful (Mimosa pudica), leaf extract: a precursor for organic electronics applications. *Sn Applied Sciences*, *2*(3), 1-8.

Baruah, S., & Dutta, J. (2009). Hydrothermal growth of ZnO nanostructures. *Science and technology of advanced materials*.

Barzinjy, A. A., & Azeez, H. H. (2020). Green synthesis and characterization of zinc oxide nanoparticles using Eucalyptus globulus Labill. leaf extract and zinc nitrate hexahydrate saltj, *2*(5), 1-14.

Biasotto, G., Ranieri, M.G.A., Foschini, C. R., Simes A. Z., Longo, E., Zaghete M. A. (2014) Gas sensor applications of zinc oxide thin film grown by the polymeric precursor method, *Ceram. Int.* 40 (2014) 14991–14996. doi:10.1016/j.ceramint.2014.06.099

Byzynski, G., Andreza, P. P., Diogo, P. V., Caue, R., Elson L. (2017). High-performance ultraviolet-visible driven ZnO morphologies photocatalyst obtained by microwave-assisted hydrothermal method, *Journal of Photochemistry and Photobiology A: Chemistry* https://doi.org/10.1016/j.jphotochem.2017.11.032

Chemingui, H., Missaoui, T., Mzali, J. C., Yildiz, T., Konyar, M., Smiri, M., ... & Yatmaz, H. C. (2019). Facile green synthesis of zinc oxide nanoparticles (ZnO NPs): Antibacterial and photocatalytic activities. *Materials Research Express*, *6*(10), 1050b4.

Chen, L., Wang, L., Wu, X., & Ding, X. (2017). A process-level water conservation and pollution control performance evaluation tool of cleaner production technology in textile industry. *Journal of cleaner production*, *143*, 1137-1143.

Cotillas, S., Llanos, J., Cañizares, P., Clematis, D., Cerisola, G., Rodrigo, M. A., & Panizza, M. (2018). Removal of Procion Red MX-5B dye from wastewater by conductive-diamond electrochemical oxidation. *Electrochimica Acta*, *263*, 1-7.

Diya'uddeen, B. H., Wan Mohd, W., Wan, A., Daud, A.R., Aziz A. (2011): Treatment technologies for petroleum refinery effluents: *A review, Process Safety and Environmental Protection*, 89 (2011) *95–105*

Golmohammadi, M., Honarmand, M., & Ghanbari, S. (2020). A green approach to synthesis of ZnO nanoparticles using jujube fruit extract and their application in photocatalytic degradation of organic dyes. *Spectrochimica Acta Part A: Molecular and Biomolecular Spectroscopy*, *229*, 117961.

Hameed, B. H, Akpan, U. G., Wee, K. P. (2011): Photocatalytic degradation of Acid Red 1 dye using ZnO catalyst in the presence and absence of silver, *Desalination and Water Treatment*, 27: 204-209

Hassani, A., Khataee, A., Karaca, S., Karaca, C., & Gholami, P. (2017). Sonocatalytic degradation of ciprofloxacin using synthesized TiO2 nanoparticles on montmorillonite. *Ultrasonics sonochemistry*, *35*, 251-262.

Huo, S., Ding, S., Zhao, C., Wang, C., Yu, F., Fang, J., & Yang, Y. (2021). Growth and Photocatalytic Activities of Porous ZnO/TiO2 Composite Microspheres with Crystalline –Amorphous Phase Boundary. *Catalysis Letters*, *151*(7), 1937-1947.

Ibrahim, N.B, AL-Shomar, S. M., Sahrim Ahmad, H. J. (2013): Effect of aging time on the optical, structural and photoluminescence properties of nanocrystalline ZnO films prepared by a sol–gel method, *Applied Surface Science 283 (2013) 599–602*

Kaliraj, L., Ahn, J. C., Rupa, E. J., Abid, S., Lu, J., & Yang, D. C. (2019). Synthesis of panos extract mediated ZnO nano-flowers as photocatalyst for industrial dye degradation by UV illumination. *Journal of Photochemistry and Photobiology B: Biology*, *199*, 111588.

Khan, W. Z., Imad, N., Madina, T., Zhibeek, M. (2014): Refinery wastewater degradation with titanium dioxide, Zinc oxide, and hydrogen peroxide in a photocatalytic reactor, *Process Safety and Environmental Protection* (2 0 1 4)

Khosravi, R., Ehrampoush, M. H., Moussavi, G., Ghaneian, M. T., Barikbin, B., Ebrahimi, A. A., & Sharifzadeh, G. (2019). Facile green synthesis of zinc oxide nanoparticles using Thymus vulgaris extract, characterization, and mechanism of chromium photocatalytic reduction. *Materials Research Express*, *6*(11), 115093.

Kumar, J. S., Bolimera, U. R., & Thangadurai, P. (2015). Direct sunlight responsive ZnO photocatalyst: Highly efficient photodegradation of methylene blue. In *AIP Conference Proceedings* (Vol. 2, No. 1, p. 030080). AIP Publishing LLC.

Kwon, D., & Kim, J. (2020). Silver-doped ZnO for photocatalytic degradation of methylene blue. *Korean Journal of Chemical Engineering*, *37*(7), 1226-1232.

Lam, S. M., Sin, J. C., Abdullah, A. Z., & Mohamed, A. R. (2012). Degradation of wastewaters containing organic dyes photocatalysed by zinc oxide: a review. *Desalination and Water Treatment*, *41*(1-3), 131-169.

Lawal, A. T. (2017). Polycyclic aromatic hydrocarbons. A review. *Cogent Environmental Science*, *3*(1), 1339841.

Lee, K.M., Lai, C.W., Ngai, K.S., Juan, J.C. (2015). Recent Developments of Zinc Oxide Based Photocatalyst in Water Treatment Technology: *A Review, Water Research* (2015), doi:10.1016/j.watres.2015.09.045.

Lupan, O., Guérin, V. M., Tiginyanu, I.M., Ursaki V. V., Chow L., Heinrich H, Pauporté (2010). Well-aligned arrays of vertically oriented ZnO nanowires electrodeposited on ITO-coated glass and their integration in dye sensitized solar cells, *Journal Photochem. Photobiol. A Chem.* 211 65–73. doi:10.1016/j.jphotochem.2010.02.004.

Marques, J., Gomes, T. D., Forte, M. A., Silva, R. F. & Tavares, C. J. (2019). A new route for the synthesis of highly-active N-doped TiO_2 nanoparticles for visible light photocatalysis using urea as nitrogen precursor. *Catalysis Today*, *326*, 36-45.

Megharaj, M., Ramakrishnan, B., Venkateswarlu, K., Sethunathan, N., & Naidu, R. (2014). Bioremediation approaches for organic pollutants: a critical perspective. *Environment International*, *37*(8), 1362-1375.

Meshram, S., Rohan, L., Shailesh, G., Shachi, N., Shirish, S., Rajeev, C. *(2011)*. Continuous flow photocatalytic reactor using ZnO–bentonite nanocomposite for degradation of phenol, *Chemical Engineering Journal, 172 (2011), 1008–1015. Immobilization*

Messih, M. A., Ahmed, M. A., Soltan, A., & Anis, S. S. (2019). Synthesis and characterization of novel Ag/ZnO nanoparticles for photocatalytic degradation of methylene blue under UV and solar irradiation. *Journal of Physics and Chemistry of Solids*, *135*, 109086.

Mhamdi, A, Labidi, A, Souissi, B., Kahlaoui, M., Yumak., Boubaker, K., Amlouk, A., Amlouk, M. (2015). Impedance spectroscopy and sensors under ethanol vapors application of sprayed vanadium-doped ZnO compounds, *Alloys Compd.* 639 648–658. doi:10.1016/j.jallcom.2015.03.205

Muhammad G. Honarmand M. and Ghanbari S. A green approach to synthesis of ZnO nanoparticles using jujube fruit extract and their application in photocatalytic degradation of organic dyes, *Spectrochimica Acta Part A: Molecular and Biomolecular Spectroscopy* (2019)

Muhammad Imran Din, Summiya Jabbar, Jawayria Najeeb, Rida Khalid, Tayabba Ghaffar, Muhammad Arshad, Safyan A. Khan & Shahid Ali (2020): Green synthesis of zinc ferrite nanoparticles for photocatalysis of methylene blue, *International Journal of Phytoremediation*

Nguyen, C. H., Fu, C. C., & Juang, R. S. (2018). Degradation of methylene blue and methyl orange by palladium-doped TiO2 photocatalysis for water reuse: Efficiency and degradation pathways. *Journal of Cleaner Production*, *202*, 413-427.

Osuntokun, J., Onwudiwe, D. C., & Ebenso, E. E. (2019). Green synthesis of ZnO nanoparticles using aqueous Brassica oleracea L. var. italica and the photocatalytic activity. *Green Chemistry Letters and Reviews*, *12*(4), 444-457.

Prabakaran, E., & Pillay, K. (2019). Synthesis of N-doped ZnO nanoparticles with cabbage morphology as a catalyst for the efficient photocatalytic degradation of methylene blue under UV and visible light. *RSC Advances*, *9*(13), 7509-7535.

Pirhashemi, M., Habibi-Yangjeh*n*, *A. (2015):* Ternary ZnO/AgBr/Ag2CrO4 nanocomposites with tandem n–n heterojunctions as novel visible-light-driven photocatalysts with excellent activity, *Ceramics International* 41 (2015) 14383–14393

Rowshon, Saifullah, Khalid, A., Ahmed, A. Z., Masum, S. M., Molla, M., & Islam, A. (2020). Synthesis of N-Doped ZnO Nanocomposites for Sunlight Photocatalytic Degradation of Textile Dye Pollutants. *Journal of Composites Science*, *4*(2), 49.

Saadati, F., Keramati, N., & Ghazi, M. M. (2016). Influence of parameters on the photocatalytic degradation of tetracycline in wastewater: a review. *Critical reviews in environmental science and technology*, *46*(8), 757-782.

Samadi, M., Zirak, M., Naseri, A., Khorashadizade, E., & Moshfegh, A. Z. (2016). Recent progress on doped ZnO nanostructures for visible-light photocatalysis. *Thin Solid Films*, *605*, 2-19.

Saravanakumar T, M., Newman, J. P., & Kubheka, O. (2020). Effect of TiO2 phase on the photocatalytic degradation of methylene blue dye. *Physics and Chemistry of the Earth, Parts A/B/C*, *118*, 102900.

Selvin, S. S. P., Radhika, N., Borang, O., Lydia, I. S., & Merlin, J. P. (2017). Visible light driven photodegradation of Rhodamine B using cysteine capped ZnO/GO nanocomposite as photocatalyst. *Journal of Materials Science: Materials in Electronics*, *28*(9), 6722-6730.

Siadatnasab, F., Farhadi, S., & Khataee, A. (2018). Sonocatalytic performance of magnetically separable CuS/CoFe2O4 nanohybrid for efficient degradation of organic dyes. *Ultrasonics sonochemistry*, *44*, 359-367.

Sinar Mashuri, S. I., Ibrahim, M. L., Kasim, M. F., Mastuli, M. S., Rashid, U., Abdullah, A. H., and Yun Hin, T. Y. (2020). Photocatalysis for organic wastewater treatment: From the basis to current challenges for society. *Catalysts*, *10*(11), 1260.

Subbiah, R., Muthukumaran, S., & Raja, V. (2019). Fine-tuning of energy gap, FTIR, photoluminescence and photocatalytic behavior of Centella asiatica extract

mediated Mn/Mg doped ZnO nanostructure. *Journal of Materials Science: Materials in Electronics*, *30*(18), 17066-17077.

Sun, L., Shao, Q., Zhang, Y., Jiang, H., Ge, S., Lou, S., & Guo, Z. (2020). N self-doped ZnO derived from microwave hydrothermal synthesized zeolitic imidazolate framework-8 toward enhanced photocatalytic degradation of methylene blue. *Journal of Colloid and interface science*, *565*, 142-155.

Tichapondwa, S. M., Newman, J. P., & Kubheka, O. (2020). Effect of TiO2 phase on the photocatalytic degradation of methylene blue dye. *Physics and Chemistry of the Earth, Parts A/B/C*, *118*, 102900.

Ullah, A. A., Kibria, A. F., Akter, M., Khan, M. N. I., Tareq, A. R. M., & Firoz, S. H. (2017). Oxidative degradation of methylene blue using Mn 3 O 4 nanoparticles. *Water Conservation Science and Engineering*, *1*(4), 249-256.

Varadavenkatesan, T., Lyubchik, E., Pai, S., Pugazhendhi, A., Vinayagam, R., & Selvaraj, R. (2019). Photocatalytic degradation of Rhodamine B by zinc oxide nanoparticles synthesized using the leaf extract of Cyanometra ramiflora. *Journal of Photochemistry and Photobiology Biology*, *199*, 11621.

Vasiljevic, Z. Z., Dojcinovic, M. P., Vujancevic, J. D., Jankovic-Castvan, I., Ognjanovic, M., Tadic, N. B & Nikolic, M. V. (2020). Photocatalytic degradation of methylene blue under natural sunlight using iron titanate nanoparticles prepared by a modified sol–gel method. *Royal Society Open Science*, *7*(9), 200 and 708.

Vermorel, N., San-Valero, P., Izquierdo, M., Gabaldón, C., & Penya-Roja, J. M. (2017). Anaerobic degradation of 2-propanol: Laboratory and pilot-scale studies. *Chemical Engineering Science*, *172*, 42-51.

Volkova, N. A., Evstrop'ev, S. K., Istomina, O. V., & Kolobkova, E. V. (2018). Photolysis of diazo dye in aqueous solutions of metal nitrates. *Optics and spectroscopy*, *124*(4), 489-493.

Wang, D., Jia, F., Wang, H., Chen, F., Fang, Y., Dong, W., ... & Yuan, X. (2018). Simultaneously efficient adsorption and photocatalytic degradation of tetracycline by Fe-based MOFs. *Journal of colloid and interface science*, *519*, 273-284.

Wang, J.P., Xu, H., Qian, X.F., Dong, Y.Y., Gao, J.K., Qian, G.D., Yao, J.M. (2015). Modification of g-C3N4 with CuO for enhanced photocatalysis. *Chemistry-Asian Journal*, 10, 1276-1280

Wang, J., Chen, R., Xia, Y., Wang, G., Zhao, H., Xiang, L., & Komarneni, S. (2017). Cost-effective large-scale synthesis of oxygen-defective ZnO photocatalyst with superior activities under UV and visible light. *Ceramics International*, *43*(2), 1870-1879.

Wang, W., Tadé, M. O., & Shao, Z. (2018). Nitrogen-doped simple and complex oxides for photocatalysis: a review. *Progress in Materials Science*, *92*, 33-63.

Ye, J., Li, X., Hong, J., Chen, J., & Fan, Q. (2015). Photocatalytic degradation of phenol over ZnO nanosheets immobilized on montmorillonite. *Materials Science in Semiconductor Processing*, *39*, 17-22.

Zewde, A. A., Zhang, L., Li, Z., & Odey, E. A. (2019). A review of the application of sonophotocatalytic process based on advanced oxidation process for degrading organic dye. *Reviews on environmental health*, *34*(4), 365-375.

Zhu, X., Pathakoti, K., & Hwang, H. M. (2019). Green synthesis of titanium dioxide and zinc oxide nanoparticles and their usage for antimicrobial applications and

environmental remediation. In *Green Synthesis, Characterization and Applications of Nanoparticles* (pp. 223-263).